Quaternary Science Reviews 358 (2025) 109353

Contents lists available at ScienceDirect

Quaternary Science Reviews

journal homepage: www.elsevier.com/locate/quascirev

Retreat of the Boothia-Lancaster ice stream from its Last Glacial Maximum extent and its role in the origin of Baffin Bay Detrital Carbonate (BBDC) events 0, 1 and 2

Anne Jennings [a,*], Kimberley Jenner [b], Alexandre Normandeau [b], Wendy Roth [a], John Andrews [a], Robert Kelleher [a], Juliette Girard [c], Brendan Reilly [d], Calvin Campbell [b], Robbie Bennett [b]

[a] INSTAAR, University of Colorado, Boulder, CO, USA
[b] Geological Survey of Canada (Atlantic), Natural Resources Canada, Nova Scotia, Canada
[c] ISMER, University of Quebec at Rimouski, Canada
[d] LDEO, Columbia University, NY, USA

ARTICLE INFO

Keywords:
Pleistocene
Holocene
North Atlantic
Glaciation
Sedimentology-marine cores
Micropaleontology-foraminifers

ABSTRACT

We combine geomorphological and sediment core evidence to investigate phases of ice margin stability and instability during retreat of the Boothia Lancaster Ice Stream (BLIS) of the NE Laurentide Ice Sheet (LIS) since the Last Glacial Maximum (LGM). Sediment cores 2008029-059 PC and TWC (59CC) and 2013029-064 PC (64 PC) from Lancaster Sound and Baffin Bay, respectively, represent LGM through Holocene environments, including three Baffin Bay Detrital Carbonate (BBDC) events that have been thought to manifest calving events within Lancaster Sound. Previous mapping of glacigenic landforms shows that 64 PC lies within the LGM limit of the convergent BLIS and Tasiujaq Ice Stream (TIS) on the northeastern Baffin Island shelf, while 59CC terminates within subglacial/ice marginal sediments termed the Baffin Shelf Drift (BSD), capturing the history of BLIS retreat from 15.3 cal ka BP onward. In 64 PC, a basal sediment gravity flow deposit is overlain by dolomite-rich BBDC 2, which is re-interpreted here as a subglacial/ice marginal deposit and renamed GZ-BBDC. Both gravity flows are interpreted to have formed during retreat of the confluent TIS and BLIS from the LGM maximum extent. Overlying GZ-BBDC, in 64 PC, is a finely laminated lithofacies interpreted as an ice-shelf facies formed beneath the ice shelf fronting the confluent TIS and BLIS when it occupied a large LGM grounding zone wedge (GZW) in northern Baffin Bay. The ice-shelf facies indicates temporary stabilization of the conjoined TIS and BLIS. The overlying thin black glaciomarine diamicton records disintegration of the ice shelf and retreat of the TIS. Ice retreat over Cretaceous and younger bedrock into Lancaster Sound is recorded by dark brown diamicton and glaciomarine sediments in 59CC. The overlying tan, detrital carbonate-rich glaciomarine diamicton, BBDC 1 in 59 PC, manifests calving retreat of the BLIS onto the Paleozoic carbonate bedrock within Lancaster Sound by 15 cal ka BP. A slightly later onset of BBDC 1 in 64 PC, of ca.14.5 cal ka BP, points to the influence of local conditions such as sea ice and local iceberg calving on the distribution of IRD off of Pond Inlet. The pause in ice rafting and detrital carbonate deposition between BBDC 1 and BBDC 0 within the Younger Dryas chron likely results from BLIS readvance to Devon Island and its stabilization there until 11.6 cal ka BP. BLIS retreat into Prince Regent Inlet marks the onset of BBDC 0. These new results indicate multiple periods of instability of the BLIS, which are responsible for BBDC events identified throughout Baffin Bay.

* Corresponding author.
E-mail addresses: anne.jennings@colorado.edu (A. Jennings), kimberley.jenner@NRCan-RNCan.gc.ca (K. Jenner), alexandre.normandeau@NRCan-RNCan.gc.ca (A. Normandeau), wendy.freeman@colorado.edu (W. Roth), andrewsj@colorado.edu (J. Andrews), Robert.Kelleher@colorado.edu (R. Kelleher), Juliette.Girard@uqar.ca (J. Girard), breilly@ldeo.columbia.edu (B. Reilly), calvin.campbell@NRCan-RNCan.gc.ca (C. Campbell), robbie.bennett@NRCan-RNCan.gc.ca (R. Bennett).

https://doi.org/10.1016/j.quascirev.2025.109353
Received 25 November 2024; Received in revised form 20 March 2025; Accepted 4 April 2025
Available online 13 April 2025

1. Introduction

Marine terminating Northern Hemiphere ice streams are subject to periods of instability and mass loss (e.g., Shaw et al., 2006; Lakeman et al., 2018; Batchelor et al., 2023), leading to episodic discharges of sediment-laden meltwater and debris-loaded icebergs into adjacent seas. These periods of mass loss can impact the Atlantic Meridional Overturning Circulation (cf. McManus et al., 2004; He and Clark, 2022), raise global sea level (cf. Alley et al., 2005; Coonin et al., 2025) and elevate sediment accumulation rates and deposition of ice-rafted debris (IRD) (cf. Okuma et al., 2024). Baffin Bay Detrital Carbonate (BBDC) events represent repeated periods of instability in ice streams terminating in northern Baffin Bay during the last glacial cycle (Aksu, 1981; Aksu and Piper, 1987; Andrews et al., 1998; Simon et al., 2012) and earlier (Hiscott et al., 1989). BBDC events are preserved in deep water in Baffin Bay as intervals of tan calcareous mud with abundant coarse clasts sourced mainly by the Boothia Lancaster Ice Stream (BLIS), which drained confluent Laurentide and Innuitian ice sheets over areas of Paleozoic carbonate bedrock via Lancaster Sound (Kelleher et al., 2022; Tremblay and Lamothe, 2022).

The youngest two BBDC events, BBDC 1 and 0, are distributed throughout Baffin Bay within a consistent deglacial age interval of ca.15 to ca.10.5 cal ka BP (Simon et al., 2014, 2016; Jennings et al., 2017; Jackson et al., 2017, 2023; Jenner et al., 2018; Kelleher et al., 2022; Ownsworth et al., 2023). These two BBDC events occurred when the BLIS had already retreated onto the Paleozoic carbonate bedrock well inside Lancaster Sound (Kelleher et al., 2022) (Fig. 1). A distinct, but unexplored break in delivery of coarse clasts and detrital carbonate is documented consistently between BBDC 1 and 0 (Jenner et al., 2018; Simon et al., 2012, 2014, 2016), but the duration of this interval is unclear, as the age of the top of BBDC 1 and base of BBDC 0 are poorly constrained. An objective of this paper is to document the timing of the inter-BBDC mud interval and understand its duration and environmental significance using paleoceanographic proxies.

Several less prominent and less well studied BBDC events were deposited prior to BBDC 1, within MIS 2 and 3; BBDC 2 and 3 of Simon et al. (2012); and BBDC 2, 3 and 4 of Jackson et al. (2023). These events also have been interpreted to indicate ice-sheet instability and calving from ice streams draining into northern Baffin Bay. However, we question whether BBDC events within the LGM, reflect similar ice extents, processes and sources to BBDC 1 and 0.

We use sediment core evidence, supported by geomorphological data, to investigate the timing, depositional processes and paleoenvironmental conditions associated with the deposition of BBDC 2, 1 and 0. Specifically, we examine two cores: 64 PC (72.426113° N; 72.769305° W; 875 mwd), from the upper slope SE of Lancaster Sound, and 59CC (74.259623° N; 82.38415° W; 791 mwd), within Lancaster Sound, to show how these events relate to deglaciation on the shelf and ice retreat into Lancaster Sound (Fig. 1). These sediment records encompass the retreat of the BLIS from the LGM position on the outer continental shelf (Li et al., 2011; Brouard and Lajeunesse, 2017) until the opening of Parry Channel to Arctic Ocean/Baffin Bay throughflow by deglaciation ca. 10.6 cal ka BP (Kelleher et al., 2022; Pieńkowski et al., 2012, 2013, 2014), and demonstrate the roles of ice shelves in modulating ice stream dynamics.

1.1. Physical setting

The physical setting of 59CC and 64 PC, including modern oceanography, bedrock geology, and glacial history in northern Baffin Bay and Lancaster Sound is detailed by Kelleher et al. (2022); only a brief synopsis is provided here.

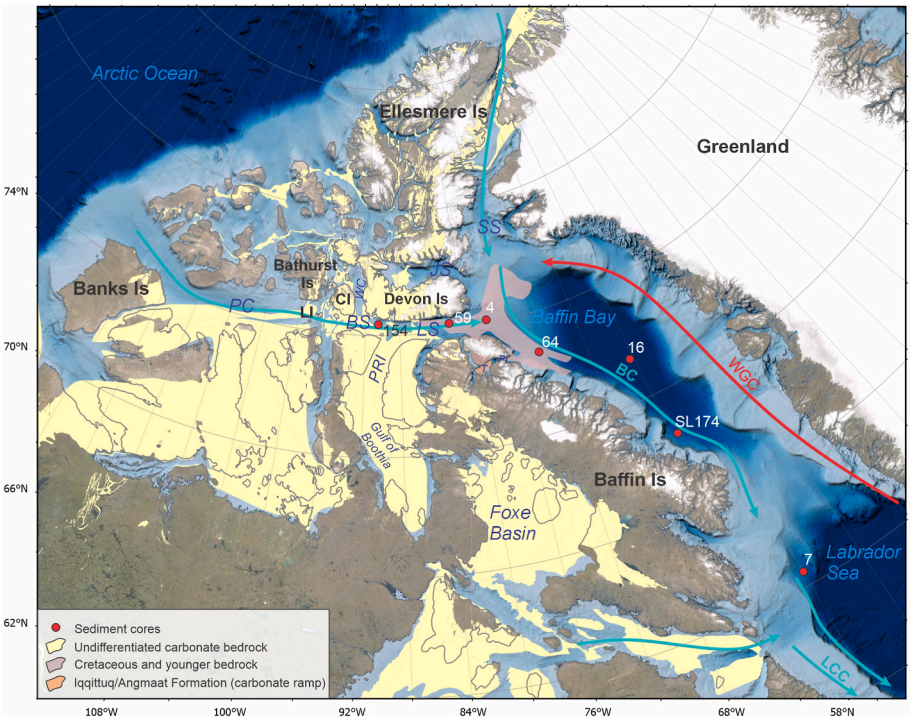

Fig. 1. Map showing study area location, distribution of key bedrock geological units (see color key) used for provenance; positions of sediment cores of this study and mentioned in the text - 59 = 2008029-59CC; 64 = 2013029-64 PC; 16 = 2008029-16 PC; 154 = 86027-154 PC; SL 174 = GeoTu SL 174; 7 = 97048-07 PC; 4 = GeoB22336-4 - and the general ocean circulation of Polar Water/Arctic Surface Water = pale blue arrows (BC = Baffin Current, LC = Labrador Current; LCC = Labrador Coastal Current) and Atlantic Water = red arrow (WGC=West Greenland Current). PC = Parry Channel; BS = Barrow Strait; WC = Wellington Channel; LS = Lancaster Sound; JS = Jones Sound; SS = Smith Sound; PRI = Prince Regent Inlet, T = Tasiujaq; PI = Pond Inlet; CI = Cornwallis Island; LI = Lowther Island. Bathymetry is from the GEBCO Compilation Group (2024), and the bedrock geology is from Harrison et al. (2011b) with some additions from Currie et al. (2020).(For interpretation of the references to colour in this figure legend, the reader is referred to the web version of this article.)

Cyclonic ocean circulation in Baffin Bay involves northward flow of the West Greenland Current (WGC), carrying warm, saline Atlantic Water along western Greenland, and southward flow of the Baffin Current, comprised of cold and low salinity Arctic Surface Water (ASW), along Baffin Island (Fig. 1) (Tang et al., 2004; Münchow et al., 2015). Arctic-sourced waters form the upper 100–300 m of surface water in Baffin Bay; warmer and more saline Atlantic Water underlies the ASW forming an intermediate water mass (300–800 m) (Tang et al., 2004). The modern sea-ice edge extends southwest to northeast, within Baffin Bay, reflecting the overall dominance of Atlantic Water (less sea ice) in the SE and Arctic water (more sea ice) in the NW (Tang et al., 2004).

Lancaster Sound forms the easternmost segment of Parry Channel, which connects the Arctic Ocean to Baffin Bay (Fig. 1). Lancaster Sound reaches depths of over 900 m at its eastern end and shallows toward Barrow Strait, finally reaching its shallowest depths of ca.125 m at the Lowther Island sill near the western end of Barrow Strait (Pieńkowski et al., 2012; MacLean et al., 2017) (Fig. 1). The land areas surrounding Lancaster Sound are dominantly Paleozoic and Mesoproterozoic carbonate and siliciclastic rocks and Archean igneous rocks and gneiss (Furze et al., 2017; Harrison et al., 2011a; Miall et al., 1980). Paleozoic strata are inferred to extend offshore along with crystalline basement rocks (Harrison et al., 2011a) (Fig. 1). Geophysical surveys indicate that Cretaceous and younger strata underlie outer Lancaster Sound, at the margins of and beneath the extensive Baffin Fan, a sediment depocenter formed during Cenozoic rifting events that opened Baffin Bay (Harrison et al., 2011a), and Pond Inlet northwestward to Tasiujaq (Currie et al., 2020) (Fig. 1). Dark brown basal diamictons lacking detrital carbonate and distinctly different in composition to the tan diamictons of BBDC 1 and 0, were recovered from sediment cores in outer Lancaster Sound; these units provide evidence that the BLIS eroded and deposited Cretaceous and younger strata when it occupied outer Lancaster Sound (Bennett et al., 2014; Kelleher et al., 2022). Bedrock drilling offshore Buchan and Scott troughs (MacLean and Falconer, 1979) recovered cores of Cretaceous bedrock comprised of dark, gray-brown siltstone consistent with the black/dark brown diamictons described in Lancaster Sound (Kelleher et al., 2022) and on the NE Baffin Slope, south of Lancaster Sound (Jenner et al., 2018). Klassen (1985) noted that the Cretaceous Tertiary sedimentary rock that underlies lowland areas of Bylot Island and NW Baffin Island are too unconsolidated to form very coarse debris in glacial deposits. The distributions and distinct mineralogical compositions and color differences between Cretaceous and younger bedrock versus Mesoproterozoic and Paleozoic carbonate bedrock provide important information for reconstructing past ice margin positions (e.g. Klassen, 1985) (Fig. 1).

1.2. Glacial history

During the LGM confluent Laurentide, Innuitian, and Greenland ice sheets filled the Arctic Island Channels (England et al., 2006) and this may have been the situation from sometime within MIS 5 (Simon et al., 2012; Andrews et al., 2024). Streaming ice from multiple outlets converged in Lancaster Sound to form the Lancaster Sound ice stream (LSIS) (MacLean et al., 2017). At the root of this large flow was the enormous Gulf of Boothia ice stream (Fig. 1). It flowed northward from Foxe Basin, toward Parry Channel, where it turned eastward and flowed down Lancaster Sound toward Baffin Bay (Fig. 1) (MacLean et al., 2017; Margold et al., 2018; Tremblay and Lamothe, 2022). Tremblay and Lamothe (2022) call this complex the BLIS, and we adopt that terminology. In Lancaster Sound, the trunk ice stream became confluent with other ice streams fed by the Foxe Dome, such as Admiralty Inlet, Navy Board Inlet and Tasiujaq (formerly Eclipse Sound/Pond Inlet ice stream) ice streams, as well as ice outlets of the Innuitian Ice Sheet (IIS), the most important being the Wellington Channel ice stream fed by ice from Cornwallis, Devon and Bathurst islands (Dyke, 1999; Dyke et al., 2002; Maclean et al., 2017; Margold et al., 2018). As evidenced by the detrital carbonate charged Eclipse Moraines on Bylot Island, and northern Baffin Island, the BLIS was grounded in Lancaster Sound, possibly reaching ice thicknesses of 1600 m as it emerged onto the Baffin Island Shelf (Klassen and Fisher, 1988; Dyke et al., 2002; MacLean et al., 2017) where it was grounded to 1300 m water depth at the LGM (Li et al., 2011; Brouard and Lajeunesse, 2017) (Fig. 2A). The Eclipse Moraines were originally thought to predate the LGM (Klassen, 1993; McCuaig, 1994) but as described by Tremblay and Lamothe (2022), more recent considerations indicate the Eclipse Moraines correspond with the LGM (Dyke and Hooper, 2001; Dyke et al., 2002).

Previous mapping of glacigenic landforms - mega-scale glacial lineations (MSGLs), GZWs and retreat moraines show that 64 PC lies within the LGM limit of the convergent BLIS and Tasiujaq ice stream (TIS) (Brouard and Lajeunesse, 2017; MacLean et al., 2017; Kelleher et al., 2022) (Fig. 2A). The presence of an ice stream in Lancaster Sound is supported by MSGLs and drumlinoid ridges mapped on the seafloor (Bennett et al., 2013; 2014; Bennett et al., 2016; Furze et al., 2017; Maclean et al., 2017). Adjacent to the BLIS were smaller LIS outlets that extended onto the eastern Baffin Island continental shelf via cross-shelf troughs (Brouard and Lajeunesse, 2017) and were fronted by large floating ice shelves during the LGM (Couette et al., 2022), and which may have governed LGM ice shelves throughout northern Baffin Bay (Batchelor et al., 2024). GZWs inboard of the LGM ice limit of these outlets suggest that fringing ice shelves formed during stillstands in the retreat of the LIS after initial LGM retreat (Bennett et al., 2013, 2014; Brouard and Lajeunesse, 2017; Furze et al., 2017; MacLean et al., 2017; Couette et al., 2022) (Fig. 2A, B, C). Two GZWs in Lancaster Sound 50–75 km west of 59 PC indicate periods of stabilization of the BLIS after retreat from the LGM position (Fig. 2A).

Based on lithofacies and ages in 59CC, the grounded ice margin had retreated well inside Lancaster Sound (west of core site 59CC) by ca.15.3 cal ka BP, prior to the onset of BBDC 1 (Kelleher et al., 2022). This constraint is not reflected in recent ice sheet (Dalton et al., 2020, 2023) and local ice margin (Okuma et al., 2023) reconstructions that show the BLIS was grounded beyond the mouth of Lancaster Sound until BBDC 1, nor during the Younger Dryas cold period where Dalton et al. (2024) map a large ice shelf extending beyond the mouth of Lancaster Sound. Data presented in this paper will expand on the evidence for extensive ice margin retreat into Lancaster Sound prior to the onset of BBDC 1.

1.3. Previous work and background on 2013029-64 PC and 2008029-59CC

2013029–64 PC was studied previously to gain an understanding of sedimentary environments and sediment sources over the last glacial cycle along the Baffin Island margin (Campbell et al., 2017; Jenner et al., 2018; Andrews et al., 2020) and during ice retreat within Lancaster Sound (Kelleher et al., 2022). Jenner et al. (2018) identified four lithofacies in 64 PC based on sedimentary structures, color, grainsize, physical properties measurements and portable X-ray Fluorescence (pXRF) data augmented by quantitative X-ray diffraction (qXRD) mineralogy (Andrews et al., 2020). We use these original lithofacies in 64 PC as a framework to investigate the glacial and paleoceanographic history using the new data presented herein (Fig. 3).

The lithofacies defined by Jenner et al. (2018) and Andrews et al. (2020), for 64 PC, begin with L1g, dark gray-brown, graded diamicton with low Ca/Ti values (713 - 587 cm), interpreted as laterally supplied sediment (i.e. from the adjacent Baffin Island margin) deposited by gravity flow processes. L1g is abruptly overlain by L3, a massive, tan calcareous, gravelly sandy mud with elevated Ca/Ti values (587 - 523 cm), attributed to ice rafting and meltwater plume deposition from Lancaster Sound, similar to other BBDC events. It was labelled BBDC 2 in Jenner et al. (2018) with the suggestion that it might be correlated to BBDC 2 in deep water Baffin Bay cores. At 550 cm L3 (BBDC 2) becomes stratified and shares a gradational contact with overlying L2 - laminated red brown mud (523 - 441 cm). The laminated mud includes some

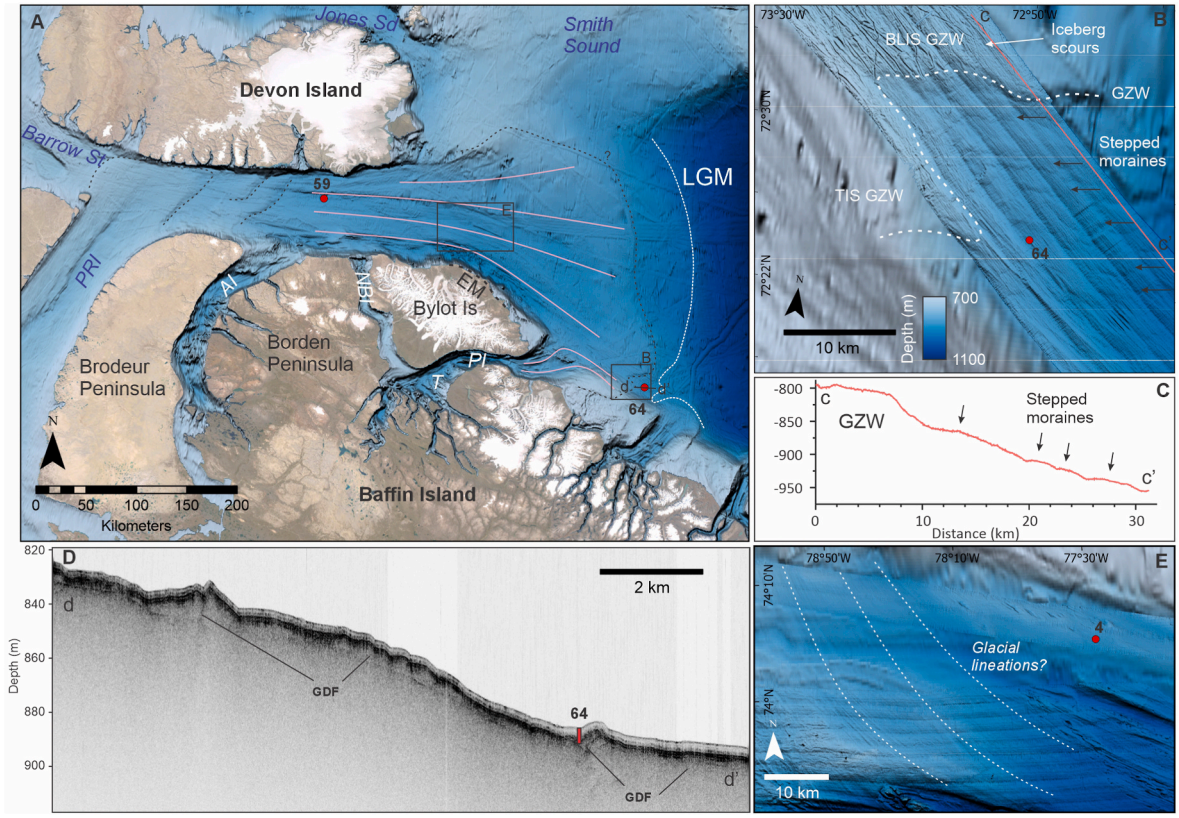

Fig. 2. A. Locations of cores 59 PC and TWC and 64 PC on bathymetric data with boxes showing location of panels B and E. PRI = Prince Regent Inlet; AI = Admiralty Inlet; NBI = Navy Board Inlet; T = Tasiujaq; PI = Pond Inlet; EM = Eclipse Moraines. Dashed black lines on bathymetry mark landforms and sediment deposited along former grounding lines. Dashed white line indicates LGM position from Li et al. (2011) and Brouard and Lajeunesse (2017). B. Closer view of the seabed around the 64 PC site showing stepped moraines to the southeast of a composite GZW deposited by confluent ice streams emanating from BLIS and TIS. Red line c-c' marks bathymetric transect shown in panel C. C. Depth transect c-c' from GZW through stepped moraines. D. Acoustic profile across d-d' showing GDFs associated with stepped retreat moraines. E. Possible glacial lineations in outer Lancaster Sound relative to core GeoB22336-4 (4).

coarser layers and dispersed clasts near the base and top of the unit and has Ca/Ti values in between those of underlying L1g and L3 (BBDC 2). L2 in 64 PC was interpreted to reflect deposition by meltwater plumes with rare iceberg rafting. In this paper we test the hypothesis that this represents an ice shelf facies (cf. Jennings et al., 2022). The transition upward from L2 to L1m - massive black diamicton (441 - 388 cm) - is marked by very low Ca/Ti values. The relatively high kaolinite content in L1m was suggested by Kelleher et al. (2022) to confirm the idea of lateral sediment supply from Cretaceous bedrock sources on the adjacent shelf (MacLean et al., 1978; Harrison et al., 2011a) or within Pond Inlet. Jenner et al. (2018) interpreted this unit as proximal glaciomarine. From 388 to 187 cm is a second occurrence of L3 – predominantly massive tan calcareous mud with high Ca/Ti values – interpreted to represent deposition from ice rafting and meltwater plumes (Jenner et al., 2018) (Fig. 3). This unit encompasses both BBDC 1 and BBDC 0 which are separated by a dark brown mottled mud layer with few dispersed clasts from 302 to 290 cm. The mud unit is clearly demarcated by its very low Ca/Ti values (Jenner et al., 2018) (Fig. 3). The top of BBDC 0 has been interpreted to mark deglaciation to the point of the opening of Parry Channel (Kelleher et al., 2022). From 187 cm to the core top is brown bioturbated mud of L4 with low Ca/Ti values reflecting postglacial hemipelagic sedimentation (Fig. 3) (Jenner et al., 2018; Kelleher et al., 2022).

2008029–59CC Although most data presented in this paper use information from 59 PC, we present this site in both PC depths and CC depths because the age model includes two dates from the TWC (Fig. 3). Composite core depths (Kelleher et al., 2022) account for the overlap between the TWC and PC. Core 59CC, from within Lancaster Sound, includes a sediment sequence beginning with L1m - massive diamicton – that corresponds to Baffin Shelf Drift (BSD) (Bennett et al., 2014). Its very dark brown to black color and mineralogy and relatively high kaolinite content of 12.8 % - reflect glacial erosion of underlying Cretaceous and younger sedimentary rock (Kelleher et al., 2022) (704 -base of PC to 638 cm PC) (834–768 cm CC) (Fig. 3). Stratified dark gray-brown glaciomarine diamicton (L1s - 638 to 580 cm PC; 768 to 710 cm CC), with elevated kaolinite and very low calcite and dolomite, overlies the BSD and represents glaciomarine sedimentation and ice margin retreat over Cretaceous and younger bedrock in outer Lancaster Sound (Kelleher et al., 2022). Massive tan calcareous diamicton (L3), comprising BBDC 1 and 0, overlies L1s with a gradual contact (Fig. 3). The transition to L3 at 580 cm PC (710 cm CC) defines the beginning of BBDC 1 which is inferred to have involved the retreat of a calving ice margin over the Paleozoic carbonate bedrock (Kelleher et al., 2022). An interval of varying sediment sources begins at 379 cm PC (508 cm CC) (Kelleher et al., 2022), with the development of greater color stratification and mottling between tan calcareous, dark brown and 'red' diamicton and mud layers (Kelleher et al., 2022) (Fig. 3). Unlike in 64 PC, the top of BBDC 1 and the base of BBDC 0 were difficult to define; new pXRF data were measured to help resolve this issue (Fig. 3). At 255 cm PC (385 cm CC) tan calcareous pebbly mud marks a return to BBDC deposition that is interrupted by a whole round core gap from 215 to 240 cm PC (445 - 370 cm CC). Above this gap is a wispy dark gray-brown sandy mud unit which ends with an IRD spike at 180 cm (PC) (310 cm CC) marking the opening of Parry Channel and the top of BBDC 0 (Kelleher et al., 2022). The overlying bioturbated mud (L4) represents postglacial conditions (Fig. 3).

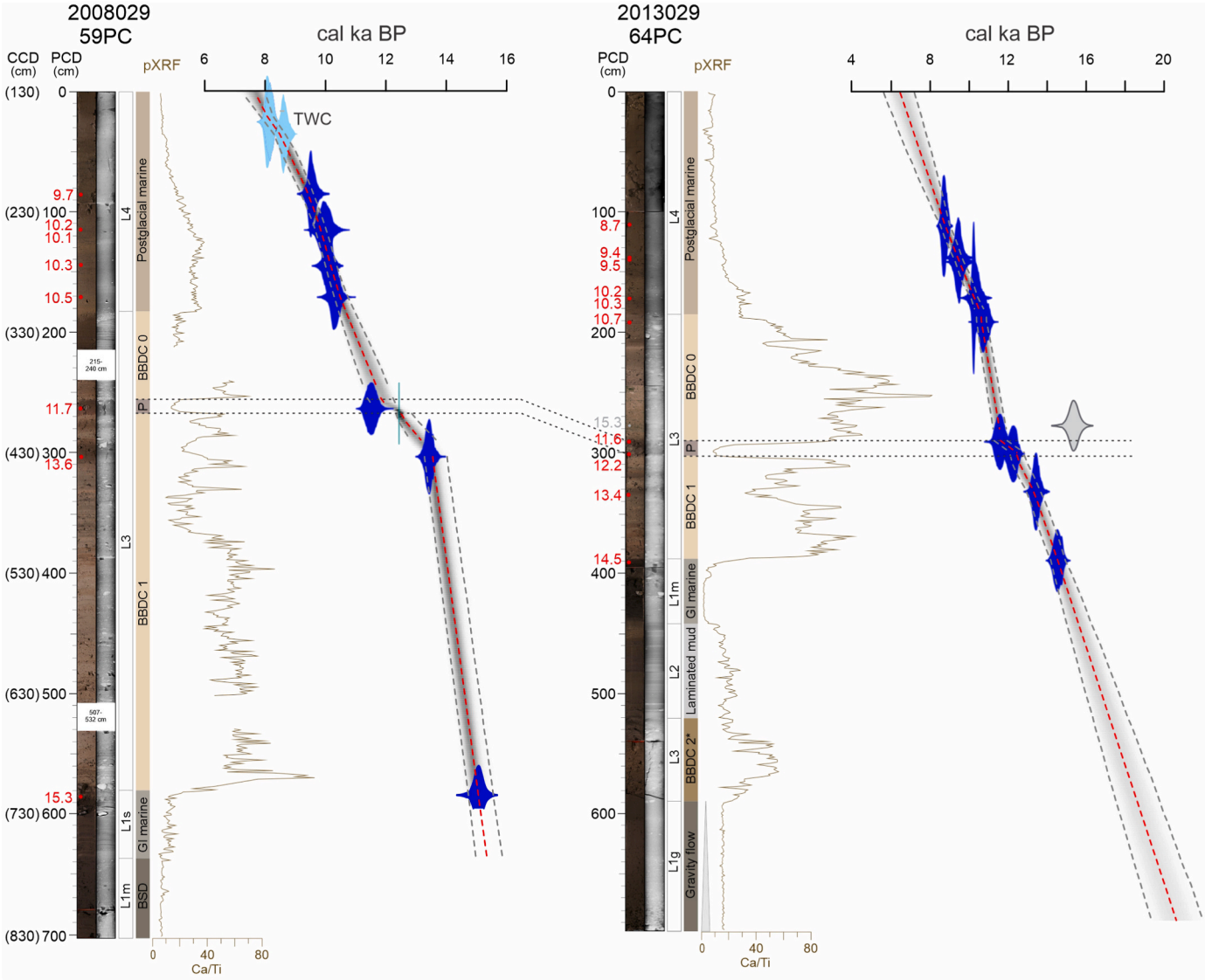

Fig. 3. From left to right, calibrated radiocarbon ages, compiled split core photography, compiled split core X-radiography, lithofacies designations and interpretations, Ca/Ti data for cores 59CC (left) and 64 PC (right). Composite TWC and PC depths were used to compile 59CC; note that light blue color denotes data from the TWC. Bayesian age-depth models with two-sigma errors are shown for each core. Light blue color refers to 59CC TWC data points. Gray age symbol denotes exclusion from age model. Green line indicates IRD pause age from 64 PC. BBDC 2* = BBDC 2 interpretation in 64 PC of Jenner et al. (2018).(For interpretation of the references to colour in this figure legend, the reader is referred to the web version of this article.)

2. Methods

Acoustic data: Multibeam bathymetry data were compiled and mosaicked from a variety of sources, including the NONNA-10 database from the Canadian Hydrographic service (https://data.chs-shc.ca/) and from Dreutter et al. (2023). These data were mosaicked with the GEBCO 2024 dataset (GEBCO Compilation Group, 2024) and represent the best available bathymetry data from the area, known to the authors as of 2024. The sub-bottom profile shown in Fig. 2 was collected during CCGS Hudson cruise 2013029 from a Knudsen 3.5 kHz sub-bottom profiler (Campbell et al., 2014)

Radiocarbon date calibration: Radiocarbon ages were calibrated using the Marine 20 database (Heaton et al., 2020) (Table 1). A Marine 20 ΔR value of 81 ± 18 ^{14}C years (Area 3, northern Baffin Bay) was applied for dates on planktonic foraminifera (Pieńkowski et al., 2022). A time varying ΔR for benthic foraminifera dates is based on 4 benthic - planktic paired dates which cover the interval between 8100 and 10200 ^{14}C yrs BP (Table 1). The benthic ΔR on each of the paired dates was calculated by subtracting the reservoir-corrected planktic age from the benthic radiocarbon age. In between these radiocarbon ages a time varying ΔR is calculated from the equation off a line forming the best fit among the 4 benthic radiocarbon ages and their benthic ΔR estimates. The equation is:

$$\Delta R_{benthic} = 0.1207 * (^{14}C\ age_{\ benthic}) - 814.4\ ^{14}C\ years$$

The maximum ΔR defined by the 4 paired dates is 414 ^{14}C years. This ΔR is applied for any benthic carbonate ages greater than 10,200 ^{14}C years. The minimum benthic ΔR defined is 164 ^{14}C years. This ΔR is applied to any benthic ^{14}C age less than 8100 ^{14}C years. An uncertainty of ±100 years is assumed for all benthic ΔR dates (Table 1). As with most ^{14}C calibrations, this approach is limited by additional uncertainties in the magnitude of ΔR that likely varied over time with locality and water depth.

Age-Depth Models: The age-depth models were constructed using rBacon, an R package that estimates the best fit or weighted mean age for each depth, with a 95 % confidence interval, using a Bayesian approach (Blaauw and Christen, 2011). However, manual inputs to the

Table 1
List of radiocarbon dates and calibrated ages from the cores in this study. Calibrated ages are based on the Marine 20 calibration curve (Heaton et al., 2020) and ΔR estimates of Pieńkowski et al. (2022) for northern Baffin Bay Area 3. Time varying benthic ΔR values are calculated from paired dates on planktonic and benthic foraminifers from the same samples.

Lab Code	Sample Code	Core	Sample interval (cm)	Sample mid-depth (cm)	CC Depth (cm)	Material Dated	Mass (mg)	Conventional 14C age (yr BP)	Error (yr)	Marine 20 Median age, yr	ΔR	ΔR (±)	σ1 Range (yr cal BP)	σ2 Range (yr cal BP)	Source
CURL-29140	GRL2055-S	2008029-59TWC	154–156	155	*155*	Planktic (Np)	3.4	8020	±35	8234	81	18	8166–8315	8066–8372	Kelleher et al. (2022)
CURL-29127	GRL2056-S	2008029-59TWC	154–156	155	*155*	MBF (Cn, In, Cr, Nl, Bf, Mb)	3.5	8110	±35	8234	164.5	100	8111–8367	7971–8483	Kelleher et al. (2022)
CURL-27419	GRL1063-O	2008029-59TWC	164–166	165	*165*	Seaweed	?	8510	±35	8818	81	18	8722–8933	8620–8993	Kelleher et al. (2022)
CURL-29132	GRL2047-S	2008029-59 PC	84–86	85	*215*	Bfs (In)	4.1	9460	±35	9692	327	100	9524–9841	9418–10048	Kelleher et al. (2022)
CURL-29125	GRL2045-S	2008029-59 PC	114–116	115	*245*	Planktic (Np)	1.5	9600	±110	10214	81	18	10053–10396	9868–10557	Kelleher et al. (2022)
CURL-29136	GRL2046-S	2008029-59 PC	114–116	115	*245*	MBF (Nl, In)	3.5	9815	±40	10105	370	100	9921–10249	9741–10437	Kelleher et al. (2022)
CURL-27441	GRL2033-S	2008029-59 PC	144–146	145	*275*	Mollusc (Pelecypod)	5	9970	±25	10300	389	100	10160–10447	9968–10600	Kelleher et al. (2022)
Beta −283442	N/A	2008029-59 PC		171	*301*	Mollusc (Tg)	?	10150	±50	10499	411	100	10308–10657	10171–10872	Bennett et al. (2015)
CURL-29138	GRL2050-S	2008029-59 PC	263–265	264	*394*	*BFs (Cn)*	7.5	11020	±40	11729	414	100	11528–11928	11318–12125	Kelleher et al. (2022)
CURL-34156	GRL-2062-S	2008029-59 PC	303–305	304	*434*	*BFs (Cn)*		12,655	±45	13590	414	100	13450–13739	13296–13902	this paper
CURL-34156	GRL-2061-S	2008029-59 PC	585–587	586	*716*	*BFs (Ec)*	4.1	13775	±40	15250	414	100	15075–15423	14915–15599	this paper
CURL-27418	GRL1066-O	2013029-64 PC	110–112	111		Seaweed	?	8435	±35	8713	81	18	8594–8805	8533–8934	Kelleher et al. (2022)
OS-118358	N/A	2013029-64 PC	135–140	137.5		MBF	2.9	9200	±35	9404	296	100	9271–9532	9095–9689	Jenner et al. (2018)
CURL-27438	GRL2037-S	2013029-64 PC	140–142	141		MBF (In, Nl, Cn)	5	9270	±25	9479	305	100	9327–9604	9189–9801	Kelleher et al. (2022)
CURL-27439	GRL2039-S	2013029-64 PC	170–172	171		Planktic (Np)	2	9615	±25	10229	81	18	10150–10298	10084–10411	Kelleher et al. (2022)
CURL-27430	GRL2038-S	2013029-64 PC	170–172	171		MBF (In, Nl, Cn, Mb + Ostracods)	6	9995	±25	10327	392	100	10187–10476	10026–10646	Kelleher et al. (2022)
CURL-27440	GRL2040-S	2013029-64 PC	190–192	191		*BFs (Cn)*	6	10300	±25	10719	414	100	10521–10892	10383–11077	Kelleher et al. (2022)

(*continued on next page*)

Table 1 (*continued*)

Lab Code	Sample Code	Core	Sample interval (cm)	Sample mid-depth (cm)	CC Depth (cm)	Material Dated	Mass (mg)	Conventional 14C age (yr BP)	Error (yr)	Marine 20 Median age, yr	ΔR	ΔR (±)	σ1 Range (yr cal BP)	σ2 Range (yr cal BP)	Source
OS-118649	N/A	2013029-64 PC	275–280	277.5		MBF	1.4	13850	±95	15347	414	100	15142–15551	14941–15762	Jenner et al. (2018)
CURL-32078	GRL-2057-S	2013029-64 PC	290–292	291		*BFs (Cn)*	5.1	10910	±35	11558	414	100	11363–11739	11221–11914	this paper
CURL-33400	GRL-2059-S	2013029-64 PC	300–302	301		*BFs (Cn)*	4	11340	±35	12225	414	100	12057–12426	11871–12564	this paper
OS-117862	N/A	2013029-64 PC	330–335	332.5		MBF	3.9	12500	±45	13414	414	100	13284–13561	13151–13709	Jenner et al. (2018)
CURL-32079	GRL2058-S	2013029-64 PC	388–392	389		Planktic (Np)	4.8	12960	±45	14525	81	18	14348–14701	14213–14835	this paper

Planktic foraminifera = Planktic; Np = Neogloboquadrina pachyderma; BFs = single species benthic foram; MBF = mixed species benthic foraminifera; species: In = Islandiella norcrossi; Nl = Nonionellina labradorica; Cr = Cassidulina reniforme; Cn = Cassidulina neoteretis; Ec = Elphidium clavatum; Mb = Melonis barleeanus; Bf = Buccella frigida; Mollusc: Tg = Thyasira gouldi = Tg; Yl = Yoldiella lenticula; Yn = Yoldiella nana. CURL = University of Colorado Radiocarbon Laboratory; OS = NOSAMS Facility, Woods Hole Oceanographic Institute; Beta = Beta Analytic Laboratory.

model were incorporated, such as defining sedimentation rates for specific intervals (boundaries) where the sedimentology and ages suggested a drastic change in sedimentation rates.

Portable X-ray fluorescence (pXRF): Data for 59 PC and 64 PC were collected using an Innov-X Delta Premium 6000 hand-held XRF, automated on a Geotek Multi Sensor Core Logger track, at 1 cm core intervals, with a 30 s dwell time per beam. pXRF was completed in Mining Plus Mode using beams one and two (40 kV, 15 kV) for 59 PC and in Soil Mode using beams two and three (40 kV. 15 kV) for 64 PC. pXRF data are reported in ppm. pXRF data were not collected from 59TWC.

Foraminiferal Assemblages: Foraminiferal assemblages in 64 PC were completed on 2 cm-long samples every 10 cm from 220 to 650 cm (47 additional samples to Kelleher et al., 2022) using the same techniques described in Kelleher et al. (2022). Subsamples were weighed, wet sieved at 63 μm, and analyzed wet in a solution of ethanol and distilled water buffered with baking soda to a pH of ca.8.4.

Quantitative X-ray Diffraction: Siltstone clasts picked from the >500 μm fractions of four foraminifera sample residues from L1m, between 390 and 432 cm in 64 PC were combined and prepared based on Eberl (2003) and tested on a Siemens D5000 X-ray Diffractometer, with a dwell time of 2 s every 0.02 two-theta between 5°–65° two-theta, generating 3000 data points. Rockjock program (Eberl, 2003) was used to calculate the weight % of 34 minerals. Mineral types were grouped according to Andrews et al. (2020). Previously published downcore qXRD mineralogy data were analyzed with the same techniques for 64 PC (to 440 cm) and 59CC in Kelleher et al. (2022). Andrews et al. (2020) presented the full qXRD mineralogy of 64 PC.

3. Results

We advance understanding of the LGM deglaciation history with new radiocarbon dates that i) improve the age models of the cores, ii) constrain the ages of the onset of glaciomarine conditions in 59CC, iii) constrain the ages of the onset and end of BBDC 1 and BBDC 0 and iv) delimit the duration of the detrital carbonate ice-rafting pause that separates BBDC 1 and BBDC 0. New pXRF data for 59CC enables further correlation between it and 64 PC and other Baffin Bay cores. Foraminiferal assemblage investigation of core 64 PC has been extended throughout its length and is supplemented with additional qXRD data to evaluate sediment provenance and thus to aid in sedimentary facies interpretations and paleoenvironmental reconstructions.

3.1. pXRF data in 59CC

New pXRF data for 59CC indicate low Ca/Ti ratios in the black and dark brown, massive (L1m) and stratified (L1s) diamictons at the base of the core (Fig. 3). A distinct rise in Ca/Ti values coincides with the onset of calcareous sediments of BBDC 1 (L3) at 580 cm PC (710 cm CC) (Fig. 3). Above 379 cm PC (508 cm CC) Ca/Ti values exhibit great variability corresponding to the color-banded interval of varying sediment source noted by Kelleher et al. (2022) (Fig. 3). In the upper part of the color-banded diamicton are three thin dark brown mud beds: 308 - 293 cm PC (438 - 423 cm CC); 280 - 275 cm PC (410 - 405 cm CC) and 255–268 cm PC (385–398 CC) with low Ca/Ti values, reflecting diminished detrital carbonate (Fig. 3). A rise in Ca/Ti values at 255 cm PC (385 cm CC) marks a return to BBDC deposition. Above the whole round core gap, the wispy dark gray brown sandy mud unit has intermediate Ca/Ti values. The overlying bioturbated mud (L4) with low Ca/Ti values represents postglacial conditions (Fig. 3) (Kelleher et al., 2022).

3.2. Updated age modeling with new ^{14}C ages

Based on abundance data revealed by foraminifera assemblage analysis, three new radiocarbon dates were acquired on 64 PC (Table 1). After additional material (388–390 cm) was prepared, the deepest

interval which had enough foraminifera for dating was from 388 to 392 cm, the top of L1m - massive black diamicton. The date was obtained from an abundance peak of the Arctic planktic foraminiferal species *Neogloboquadrina pachyderma*. This age is calibrated to 14.5 ka BP (14.4–14.7 ka 1 σ and 14.2–14.8 ka 2 σ) (Table 1) and is a close maximum-limiting constraint on the start of BBDC 1 in 64 PC (Fig. 3).

Two new dates were acquired near the base and the top of the 290–302 cm mud unit with low Ca/Ti ratios and few IRD clasts between BBDC 1 and BBDC 0 (Fig. 3). Both dates were measured on the benthic foraminifera species *Cassidulina neoteretis,* which occurs in high abundances within the mud unit. The upper date, two cm from the top of the mud unit at 290–292 cm, calibrates to 11.6 ka BP (11.4–11.7 ka 1 σ; 11.2–11.9 ka 2 σ). The lower date is from 300 to 302 cm at the base of the mud unit and calibrates to 12.2 ka BP (12.1–12.4 ka 1 σ; 11.9–12.6 ka BP 2 σ). These two dates do not overlap at one sigma and barely overlap (by 43 years) at two sigma (Table 1). Taken at face value, the dates suggest that the 12 cm mud unit represents a slowdown in sedimentation associated with reduced iceberg rafting and detrital carbonate delivery between BBDC 1 and BBDC 0 and this is reflected in the age model (Fig. 3). The age model is extended linearly from the slope of the two lowest ages to the base of the core so that the data can be plotted against age, regardless of the large uncertainties and inappropriateness of applying ages to the lower lithofacies.

Two new radiocarbon dates on benthic foraminifera were acquired from 59 PC (Table 1). A date on excellently preserved benthic foraminifera, *Elphidium clavatum* from 585 to 587 cm in the PC (715–718 cm CC), within the upper part of the dark brown glaciomarine sediments 5 cm below the base of BBDC 1, is calibrated to a median age of 15.3 ka BP, with one and two sigma age ranges of 15.1–15.4 and 14.9–15.6 ka BP, respectively. This date was measured to constrain the timing of ice retreat from the Cretaceous and younger bedrock in outer Lancaster Sound and onto the Paleozoic carbonate bedrock, marking the onset of BBDC 1. A date on *C. neoteretis* from 303 to 305 cm in 59 PC (433–435 cm CC) was measured from the lowermost of the 3 mud layers in the color stratified interval of BBDC 1 (Fig. 3). It returned a median calibrated age of 13.6 ka BP with one and two sigma age ranges of 13.5–13.7 and 13.3–13.9 cal ka BP, respectively (Table 1). This age overlaps at one sigma with the age of 13.4 cal ka BP in 64 PC, also from the lowest mud layer within the upper BBDC 1 interval, with one and two sigma age ranges of 13.3–13.6 and 13.2–13.7 cal ka BP, respectively, on *C. neoteretis* (Fig. 3). The overlap in ages at one sigma indicates that these two mud layers are time equivalent (Fig. 3).

A previously published radiocarbon age of 11.7 cal ka BP on *C. neoteretis* with one and two sigma age ranges of 11.5–11.9 and 11.3–12.1 ka from 263 to 265 cm (within the upper mud layer from 256 to 268 cm in 59 PC (386–389 cm CC) (Kelleher et al., 2022) (Table 1) matches the age of the mud layer that separates BBDC 1 and BBDC 0 in 64 PC (Fig. 3). In addition, the foraminiferal assemblages in these mud units of both cores are very similar, including the presence of unusually large and abundant *C. neoteretis* (Fig. 4). The close match between the stratigraphy and the dating of the mud layers in these two cores provides confirmation of the top of BBDC 1 at 268 cm (398 cm CC) and the base of BBDC 0 at 256 cm PC (386 cm CC) in core 59CC (Fig. 3). When constructing the age model for 59CC we assumed that the mud layers in the two cores are correlative (Fig. 3). We applied the ages of the top and base of the mud unit estimated from Bayesian age modeling in 64 PC to the top and base of the equivalent mud unit in 59CC prior to Bayesian age modeling. This approach produces a slowdown in sedimentation in 59CC associated with the low Ca/Ti ratios and the reduced delivery of detrital carbonate IRD. Linear extension of the age model from the date on *E. clavatum* in the top of L1s, downward to the base of the stratified dark brown diamicton overlying the BSD, gives an estimated age of 15.3 cal ka BP for ice retreat from the site of core 59 PC (Fig. 3).

3.3. Foraminiferal assemblages

Foraminiferal assemblages in 64 PC were completed to improve our understanding of the paleoenvironments from the LGM through to the deposition of BBDC 0 and to find intervals for additional radiocarbon dating (see above). Two extra samples (294–296 cm and 396–398 cm) were analyzed to better capture assemblages changes around lithofacies boundaries. Samples from 210 cm and higher were published in Kelleher et al. (2022) as was the foraminifera stratigraphy of 59CC. Fig. 4 shows the foraminifera abundances and species assemblages against lithofacies of the entirety of 64 PC. Of the 47 new samples, 23 had too few (<50 cutoff) foraminifera to calculate percentages (Fig. 4).

Three samples (590 cm, 620 cm and 650 cm) within the deepest lithofacies of 64 PC, L1g, graded diamicton (713–587 cm; Fig. 3) had >50 foraminifera (<68 specimens) amounting to 1 to 2 foraminifera per gram of dry sediment. The relatively large number of species, including

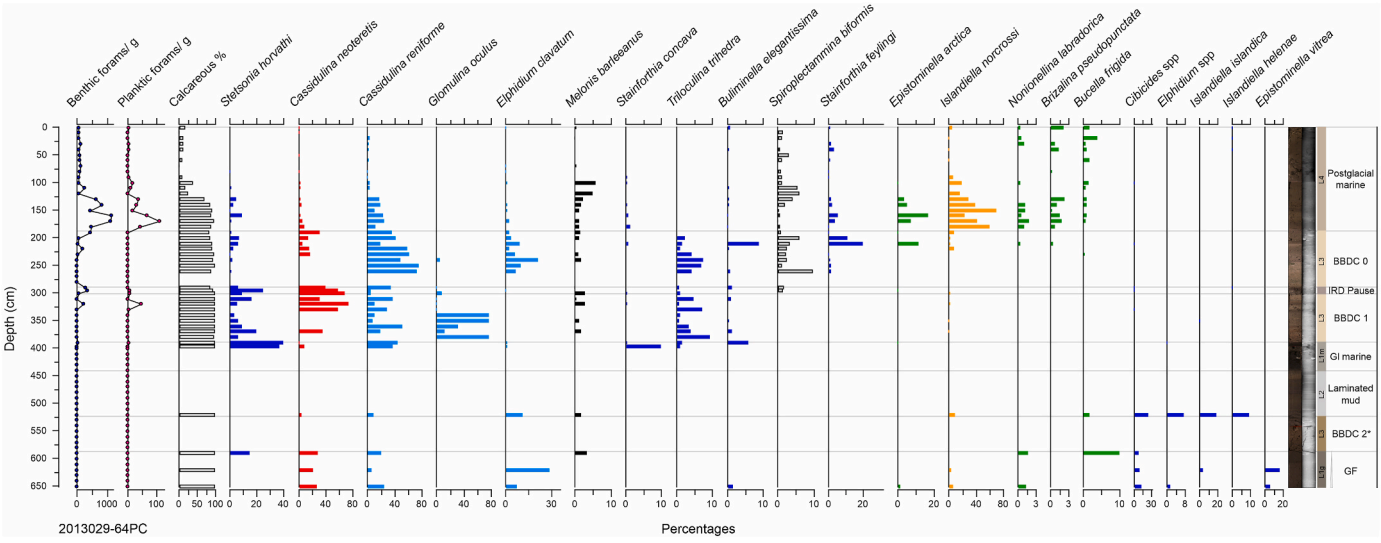

Fig. 4. Foraminiferal assemblage data for 64 PC color coded for environmental significance in this context. Navy blue bars denote Arctic or indifferent species; red bars = Atlantic species; light blue bars = glaciomarine species; black bars = buried organic matter; white bars = agglutinated species; green bars = relative increased marine productivity; orange bars = modified Atlantic Water species. Samples with fewer than 60 benthic specimens in a sample had no percentage calculation. BBDC 2* = BBDC 2 interpretation in 64 PC of Jenner et al. (2018).(For interpretation of the references to colour in this figure legend, the reader is referred to the web version of this article.)

the planktonic foraminifera *N. pachyderma*, the mixture of various environmental preferences of species, and the presence of species that are not found in samples higher in the core, suggest that these are mixed assemblages possibly reworked from older Pleistocene interglacial and interstadial deposits (cf Feyling Hanssen, 1976). This interpretation is consistent with the interpretation of this unit as a sediment gravity flow deposit (Jenner et al., 2018).

All six of the samples in L3, BBDC 2 (587–523 cm) were barren of foraminifera (containing from 1 to 16 specimens) amounting to 0 to 1 specimen per gram of dry sediment. As it is unusual for an iceberg rafted unit to be barren of foraminifera - compare for example against the faunal data in BBDC 1 and 0 - the faunal data are inconsistent with the original interpretation of L3 and support the interpretation of subglacial-ice marginal sedimentation.

Of the 8 samples analyzed in L2, laminated facies (523–441 cm) only the deepest sample had >50 foraminifera (54 specimens). This assemblage resembles the reworked assemblages in underlying L1g - graded diamicton. Upward in L2, foraminifera are extremely rare but are consistent with *in situ* production in a low productivity environment such as a sub ice-shelf environment (cf. Jennings et al., 2020a). The samples include only well preserved, fragile calcareous and agglutinated foraminifers that do not show signs of reworking such as fragmentation. Although the specimens are well preserved and likely *in situ*, the samples are considered to be barren because there are so few foraminifera.

A major transition in foraminifera assemblages and abundances occurs at the top of L1m, massive black glaciomarine diamicton (441 - 388 cm). Seven samples were analyzed and found to be barren until the upper 10 cm (396 cm) where foraminifera are abundant (47 foraminifers per gram of dry sediment) and small specimens of the planktic species *N. pachyderma* were sufficient for a radiocarbon date (^{14}C date on Np 388–392 cm, calibrated to median 14.5 ka BP; Table 1). *Stetsonia horvathi* and *C. reniforme* are the dominant benthic species in this sample, indicating heavy sea-ice cover and glaciomarine conditions (Jennings et al., 2020a).

None of the 8 samples analyzed in BBDC 1 of L3 (388 - 302 cm) is barren. Abundances range from 2 to 214 benthics per gram of dry sediment and 0 to 45 planktics per gram of dry sediment and change dramatically at 330 cm and above. *C. neoteretis* and *C. reniforme* dominate above 330 cm indicating the presence of chilled Atlantic Water (Jennings et al., 2020a). *Glomulina oculus*, a species common in high Arctic glaciomarine environments with marine terminating glaciers, is dominant below 330 cm (Jennings et al., 2020b). Perennial sea-ice cover species, *S. arctica,* is common over the full interval, while *E. clavatum*, a common glaciomarine species intolerant of perennial sea-ice cover, is absent (Jennings et al., 2020a).

Three samples were analyzed for foraminifera in the mud unit, with rare IRD, between BBDC 1 and BBDC 0 (302–290 cm). The foraminiferal assemblages are a continuation of the assemblage characteristics in the upper part of BBDC 1. These samples form an abundance peak of over 300 benthic foraminifers per gram of dry sediment and a small peak in planktic foraminifers of 7 *N. pachyderma* per gram of dry sediment. *C. neoteretis*, the dominant species, provided material for two ^{14}C dates in the lower and upper of the three samples (Figs. 3 and 4). The *C. neoteretis* were unusually large in the upper of the two ^{14}C date samples within the IRD pause. *S. arctica* is common while *E. clavatum* is absent. Together the assemblages indicate a stratified water column with heavy sea-ice cover over chilled Atlantic Water.

The first two samples within BBDC 0 (280 cm and 270 cm) are barren but overlying samples show increased numbers of benthic foraminifera per gram of dry sediment, ranging between 6 and 190. Planktic foraminifera occur in very low abundances of 1 foraminifera per gram of dry sediment in 2 samples. The dominant benthic foraminifera species are *C. reniforme* and *E. clavatum*, consistent with a glaciomarine environment with glacial meltwater but not heavy sea-ice cover (Vilks, 1980; Jennings et al., 2020a). Agglutinated foraminifera begin to increase (*Spiroplectammina biformis*). *C. neoteretis* is common and *S. arctica* occurs in low percentages. Several species that appear or increase at the top of BBDC 0 indicate marked paleoceanographic changes; *Epistominella arctica* indicates mobile sea ice and *Nonionellina labradorica* and *Brizalina pseudopunctata* indicate increased marine productivity as indicated by Kelleher et al. (2022) (Fig. 4).

Benthic and planktic foraminifera reach abundance peaks in the postglacial bioturbated marine mud described by Jenner et al. (2018) and Kelleher et al. (2022). The faunal assemblages change to high *Islandiella norcrossi* and entrance of marine productivity species associated with the opening of Parry Channel and early postglacial high marine productivity (Fig. 4). By 100 cm the faunal abundances decline as calcareous foraminifera are poorly preserved and agglutinated species dominate the assemblages. This change has been associated with the opening of Nares Strait and the transition toward modern paleoceanographic conditions (Kelleher et al., 2022).

3.4. Quantitative X-ray diffraction mineralogy

Quantitative X-ray diffraction analyses of the dark gray brown siltstone clasts were done to define the mineralogy of sedimentary bedrock inferred to be glacially eroded from lateral supply such as Cretaceous and younger mudstone in Tasiujaq/Pond Inlet (Fig. 1).

Significant weight percentages of chert, illite, and kaolinite and low amounts of calcite and dolomite, comprise the siltstone clasts of L1m immediately below BBDC 1 in 64 PC (Fig. 5). The elevated weight percentages of kaolinite and chert, along with coal pieces observed in 64 PC, therefore, seem likely to have been emplaced by glacial erosion of Cretaceous and younger sedimentary bedrock, adjacent to the core site, from Bylot Island, Tasiujaq and/or Pond Inlet (Harrison et al., 2011a; Currie et al., 2020) (Figs. 6 and 7A).

In core 59 PC the dark brown color and low Ca/Ti values in the BSD, L1m, indicate no contribution from erosion of the Paleozoic carbonate bedrock in Lancaster Sound during ice retreat from outer Lancaster Sound (Fig. 3). The elevated kaolinite content and low Ca/Ti values in the stratified diamicton, L1s, in 59CC (638 - 580 cm PC; 768 - 716 cm

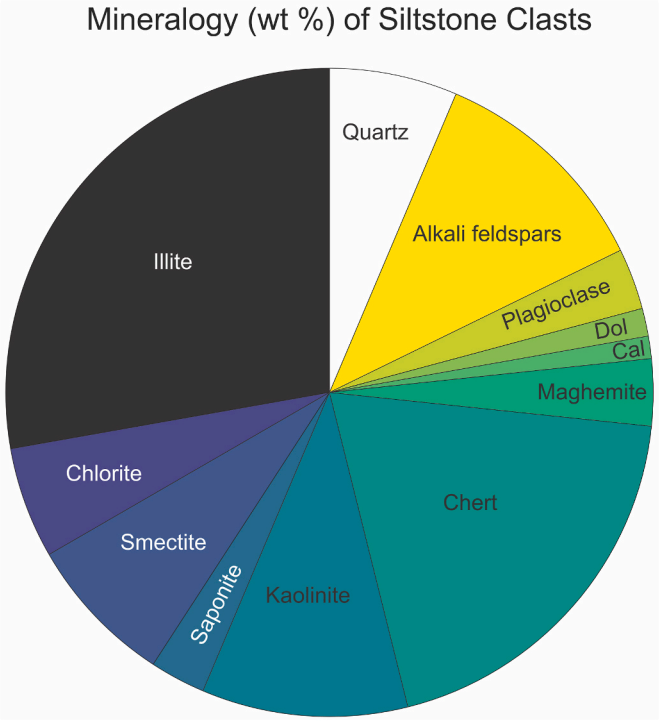

Fig. 5. Mineral weight percentages from qXRD of >500 μm siltstone clasts picked from foraminifera sample residues from L1m, in the interval between 390 and 432 cm in 64 PC.

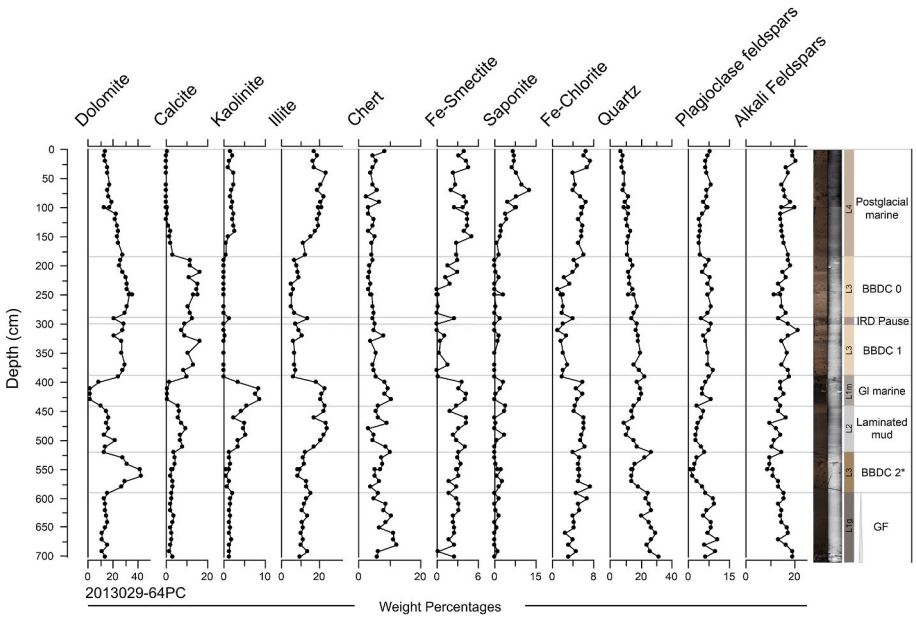

Fig. 6. Downcore mineral weight percentages from qXRD analyses in 64 PC against lithofacies. BBDC 2* = BBDC 2 interpretation in 64 PC of Jenner et al. (2018).

CC) reflect glacial erosion of Cretaceous and younger mudstone and Archean rocks (Fig. 7B). It is likely that the elevated biogenic silica found in the dark brown/black diamicton units in both 59CC and 64 PC, marks the presence of chert, shown to be common in the siltstone clasts (Fig. 5), which is more consistent with their interpreted ice marginal and subglacial origins (Kelleher et al., 2022), rather than of contemporaneously produced biogenic silica.

In 64 PC, the deepest L3 unit, BBDC 2, has low calcite and high dolomite content and a darker brown color, when compared with the upper L3 units of tan calcareous sandy gravelly mud of BBDC 1 and 0, suggesting some differences in the depositional processes and/or sediment provenance of GZ-BBDC (Figs. 6 and 7A). In contrast to BBDC 1 and 0, BBDC 2 contains Fe chlorite, slightly increased chert and kaolinite signals and lower quartz suggesting contributions from Cretaceous and younger bedrock as well as Mesoproterozoic dolostone and Paleozoic carbonate rocks (Fig. 6).

Lithofacies L2 - laminated mud - exhibits a mixed source signal including detrital carbonate (calcite and dolomite) and kaolinite (Fig. 6). The mixed signal suggests combined lateral sediment supply from Pond Inlet and Tasiujaq, Paleozoic carbonate from Lancaster Sound and northern Borden Peninsula, and Mesoproterozoic carbonate and dolostone from northern Bylot Island, northern Borden Peninsula and Tasiujaq.

BBDC 1 and 0 have essentially no kaolinite and very low Fe chlorite. However, there is a minor peak in these minerals within the mud layer between BBDC 1 and 0, which may reflect better expression of the mineralogy of background sedimentation in the absence of the dominant detrital carbonate, similar to the mineralogy of the postglacial marine mud, L4 (Fig. 6).

3.5. *Ice stream sources, sedimentary processes and paleoenvironments of 64 PC lithofacies*

We use the combined data from qXRD, foraminifera, the new age model for 64 PC, and correlations with the stratigraphy in 59CC to interpret the origins of the lithofacies in 64 PC (Figs. 3 and 7A) (Campbell and de Vernal, 2009; Campbell, 2014; Campbell et al., 2017). Unit lower and upper boundary ages are from the age-depth models. These age-depth data can be found in Jennings et al. (2025).

3.5.1. *Basal diamicton, L1g, 713-587 cm (LGM or younger)*

Jenner et al. (2018) interpreted this unit as a fining upward gravity flow deposit within a glacier dominated environment. It was deposited prior to L3 (BBDC 2), but the contact between L1g and L3 is not abrupt and suggests no period of erosion or hiatus between the two units. We interpret this unit to represent gravity flow processes associated with emplacement of the retreat moraines, with a dominance of TIS sediment sources. Its mineralogy reflects laterally supplied sediments from Pond Inlet including the Cretaceous and younger mudstone and Archean rocks and no contribution from Paleozoic carbonate rocks. The deposit is local, not appearing in adjacent cores (Jenner et al., 2018). The few foraminifera are of mixed environmental significance consistent with reworked sediments (Figs. 4 and 7A).

3.5.2. *Dolomite-rich diamicton, GZ-BBDC of L3, 587 to 523 cm (LGM or younger)*

Although BBDC 2 of Jenner et al. (2018) was originally interpreted as a glaciomarine diamicton, the research presented herein suggests a different origin. This unit is barren of foraminifera and is darker in color than later L3, BBDC events. The sub-bottom profile in Fig. 2D shows that core 64 PC penetrates through the upper conformable unit into the glacigenic debris flow deposits that form the stepped moraines (Fig. 2B and C). We reinterpret BBDC 2 as an ice marginal and/or subglacial diamicton deposited in the grounding zones of the confluent BLIS and TIS as they were retreating toward Lancaster Sound from their maximum positions on the margin (Figs. 2 and 7A). This unit is renamed GZ-BBDC to indicate that it is a grounding zone deposit rich in detrital carbonate. Stratification in the upper 15 cm is consistent with settling from debris flow processes and transition to floating ice (Fig. 3). This type of deposit is found within grounding zone wedges where ice marginal and subglacial deposits can be redistributed by gravity-flow processes (cf. Batchelor and Dowdeswell, 2015; Hogan et al., 2020). The site of 64 PC within the field of retreat moraines mapped south of the large GZW is supportive of this interpretation (Fig. 2). The stepped profiles of the retreat moraines and their acoustic transparency are characteristics of glacigenic debris flows (GDFs) associated with GZWs (Hogan et al., 2020). The darker color likely reflects the admixture of TIS and BLIS sources, with high dolomite content likely reflecting a dominantly BLIS pathway although there may also be contributions of dolomite from the Mesoproterozoic Bylot Supergroup of Tasiujaq (Jackson, 2000; Currie et al., 2020).

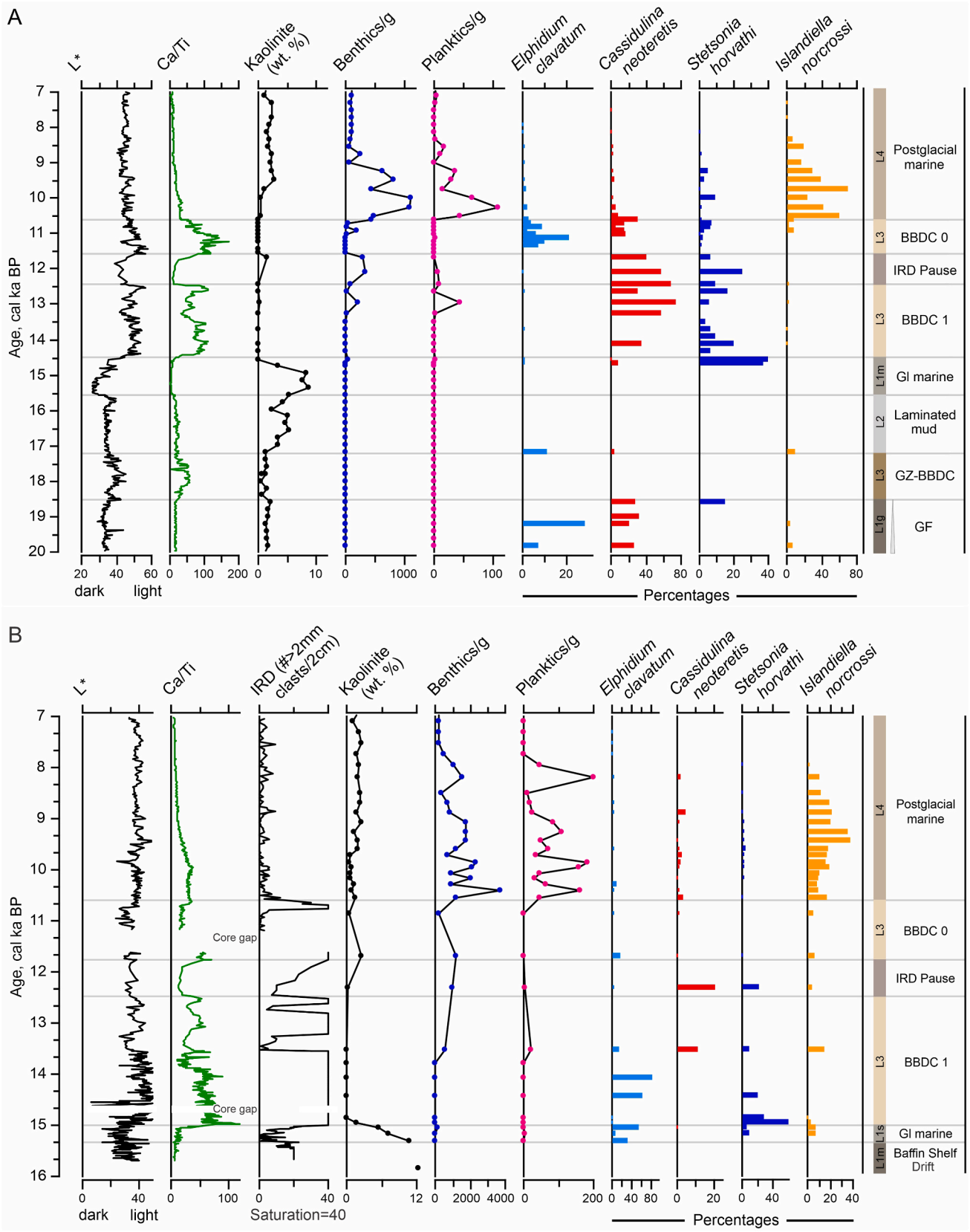

Fig. 7. Key downcore paleoenvironmental proxies against calibrated radiocarbon ages in 64 PC (A) and 59CC (B). Data in 59CC were presented in Kelleher et al. (2022) except for the Ca/Ti data which were acquired for this paper. Counts of >2 mm clasts were not completed for 64 PC.L* refers to the CIE (Commission Internationale de l'Éclairage) color space representing perceived lightness ranging from 0 = black to 100 = white. Refer to Fig. 4 caption for foraminiferal assemblage color coding.

3.5.3. Laminated mud, L2, 523 to about 441 cm (ca.17.2 - ca.15.6 cal ka BP)

The good preservation and low abundance of foraminifera in the laminated unit suggest that they likely are *in situ* and represent a low productivity, low energy environment. The mixture of detrital carbonate and kaolinite suggests combined sediment pathways from TIS and BLIS. The lack of bioturbation, rare clasts except in layers near the lower and upper boundaries, and the very low foraminiferal content supports a sub ice-shelf origin for the laminated unit (cf. Jennings et al., 2020a, 2022). The laminations probably represent deposition from sediment-charged meltwater plumes whereas the clast layers indicate release of coarse glacigenic material from the ice shelf, possibly from basal ice that was incompletely depleted of debris by melting in the grounding zone. The contact between GZ-BBDC and the laminated unit is indistinct/gradual over several centimetres, indicating that the grounding zone retreated from the site and was replaced by a sub ice-shelf environment rather than by a calving ice margin.

3.5.4. Black diamicton, L1m, 441-388 cm (ca.15.6–14.5 cal ka BP)

The black glaciomarine diamicton is barren of foraminifera until the upper 10 cm of the unit, where a radiocarbon date of 14.5 cal ka BP (14.2–14.8 cal ka BP 2 σ) on *N. pachyderma* was acquired. The benthic assemblages suggest sea-ice cover and chilled Atlantic Water. Its mineralogy reflects glacial erosion of Cretaceous and younger bedrock by the TIS, although some component of Cretaceous and younger sediment contributions from ice retreat in Lancaster Sound cannot be ruled out. We interpret this unit to reflect glaciomarine sedimentation formed by separation of the confluent ice streams, disintegration of the ice shelf and calving retreat of the TIS into Pond Inlet. This unit is chronostratigraphically correlated to the two basal units in 59CC, L1m - massive diamicton of BSD - and L1s - stratified dark gray brown glaciomarine diamicton. These two units mark retreat of the BLIS over the Cretaceous and younger bedrock (BSD) and the onset of glaciomarine sedimentation as the ice margin retreated from the site of 59CC, closely dated to 15.3 cal ka BP (Fig. 7B).

3.5.5. Detrital carbonate-rich diamicton, BBDC 1 of L3, 388 to 302 cm (14.5–12.4 cal ka BP)

The onset of BBDC 1 at 14.5 cal ka BP (2 σ range = 14.1–14.9 cal ka BP), is marked by an increase in foraminifera and a distinct color and compositional change from the black glaciomarine diamicton to detrital carbonate-enriched glaciomarine diamicton. Ca/Ti ratios are elevated throughout, but especially so from ca 14.5 to 13.4 cal ka BP, coinciding with foraminiferal faunas indicative of glaciomarine conditions, marine terminating glaciers (Figs. 4 and 7A) and a higher sedimentation rate (Fig. 3). Between ca 13.4 and 12.7 cal ka BP Ca/Ti values are lower and more variable coinciding with lower sedimentation rates (Fig. 3); the three mud units (Fig. 3) and foraminiferal faunas (Fig. 4) are indicative of ice-distal to marine conditions (Fig. 7A). The top of BBDC 1 is delineated by a distinct Ca/Ti peak estimated to have been deposited from 12.4 to 12.6 cal ka BP (Fig. 7A), (12.1–13 cal ka BP at 2 σ age range).

In 59CC, the new age model (Fig. 3) and sediment core proxies against age (Fig. 7B) indicate that BBDC 1 was first deposited circa 15 cal ka BP (2 σ range = 14.7–15.5 cal ka BP), ca.500 years earlier, in terms of mean and median modeled age, than in 64 PC (Figs. 7 and 9). BBDC 1 onset in the two cores overlaps by 200 years at two sigma, suggesting that variations in the marine reservoir age estimations could explain the apparent age difference. Similar to 64 PC, this core records a lower sedimentation rate beginning in the upper part of BBDC 1, ca 13.6 cal ka BP, which includes the color-stratified diamicton deposited from mixed sediment sources (Kelleher et al., 2022) and the 3 mud layers that are also present in 64 PC (Fig. 3). As in 64 PC, the top of BBDC 1 is defined by a peak in Ca/Ti values and increased detrital carbonate IRD (Fig. 7B).

3.5.6. IRD pause mud unit between BBDC 1 and BBDC 0 of L3, 302 to 290 cm (12.4–11.6 cal ka BP)

This foram-rich brown mud unit represents a pause in iceberg rafting of Paleozoic carbonate from the BLIS, and a slowdown in sedimentation, suggesting stabilization of the ice margins in Lancaster Sound during the Younger Dryas cold period. Foraminiferal assemblages indicate subsurface Atlantic Water and sea-ice cover (Figs. 3 and 7A). A correlative mud layer is identified in 59CC with modeled ages of 12.5 to 11.8 cal ka BP (Figs. 3 and 7B).

3.5.7. Detrital carbonate-rich diamicton BBDC 0, L3, 290 to 187 cm (11.6–10.6 cal ka BP)

This calcareous glaciomarine diamicton represents resumption of BLIS calving with a marked increase in sedimentation rate (Fig. 3), suggesting ice retreat within Lancaster Sound ending with the opening of Parry Channel to Arctic Ocean/Baffin Bay throughflow as detailed in Kelleher et al. (2022). The onset of BBDC 0 in 59CC is correlated to the top of the IRD pause mud unit with a modeled age of 11.8 cal ka BP. The termination of BBDC 0 defined at 10.6 cal ka BP (Kelleher et al., 2022), marks the final deglaciation of Parry Channel which was followed by postglacial marine mud deposition (Kelleher et al., 2022) (Fig. 7).

4. Discussion

The marine stratigraphic and geomorphological data presented here enable a comprehensive reconstruction of the deglacial dynamics of the BLIS from the LGM - when it was a conduit for convergent glaciers of the TIS and IIS - to the late-glacial - when it retreated completely from Parry Channel (Fig. 8). This reconstruction complements the terrestrial based reconstruction of Tremblay and Lamothe (2022) and constrains deglacial ice marginal positions for the NE LIS, which can be used to update published continental-scale ice sheet reconstructions (cf. Dalton et al., 2023, 2024). The results indicate a series of events depicted in Fig. 8: i). Ice retreat from the LGM position on the upper slope/outer shelf (Fig. 8A); ii) Formation of an ice shelf fronting the confluent BLIS and TIS (Fig. 8B); iii) Separation of these ice streams, ice-shelf breakup and retreat of grounded ice from the Cretaceous and younger bedrock into Pond Inlet and Lancaster Sound (Fig. 8C); iv) Deposition of BBDC 1 as grounded ice retreated on the Paleozoic carbonate bedrock within Lancaster Sound and Prince Regent Inlet (Fig. 8D); v) Readvance of the Boothia component of the BLIS out of Prince Regent Inlet to Devon Island, ending BBDC 1, and stabilization of the ice margin at Devon Island resulting in reduced IRD and Paleozoic carbonate sediment flux (IRD pause mud) (Fig. 8E); vi) Deposition of BBDC 0 during renewed retreat of the BLIS into Prince Regent Inlet and the Gulf of Boothia (Fig. 8F).

4.1. Retreat from the LGM

The sediment facies in core 64 PC begin with two debris flow deposits: L1g and L3 (GZ-BBDC), the latter of which we reinterpret here as ice marginal deposits from the confluent TIS and BLIS during the LGM. These facies have attributes of GDFs consistent with the location of the core within a field of stepped retreat moraines (Fig. 2B).

The confluent BLIS and TIS grounding zone is ca.175 km from the nearest outcrop of dolostones of the Mesoproterozoic Bylot Supergroup within Tasiujaq and ca.350 km from the Paleozoic outcrop within Lancaster Sound. This observation suggests continental scale of sediment dispersal by the BLIS, like the Home Bay Ice Stream (Tippett, 1985; Clark, 1987). The high dolomite content of GZ-BBDC suggests a long subglacial dispersal pathway that was active over an extended time period, that finally ended with retreat of the ice stream after the LGM (Clark, 1987). The high carbonate content of GZ-BBDC LGM ice-contact sediments is consistent with the high carbonate content of the Eclipse Moraines on Bylot Island (Klassen, 1993) which has similarly been correlated to the LGM extent of the BLIS (Tremblay and Lamothe, 2022).

Although the stepped retreat moraines and associated GZ-BBDC

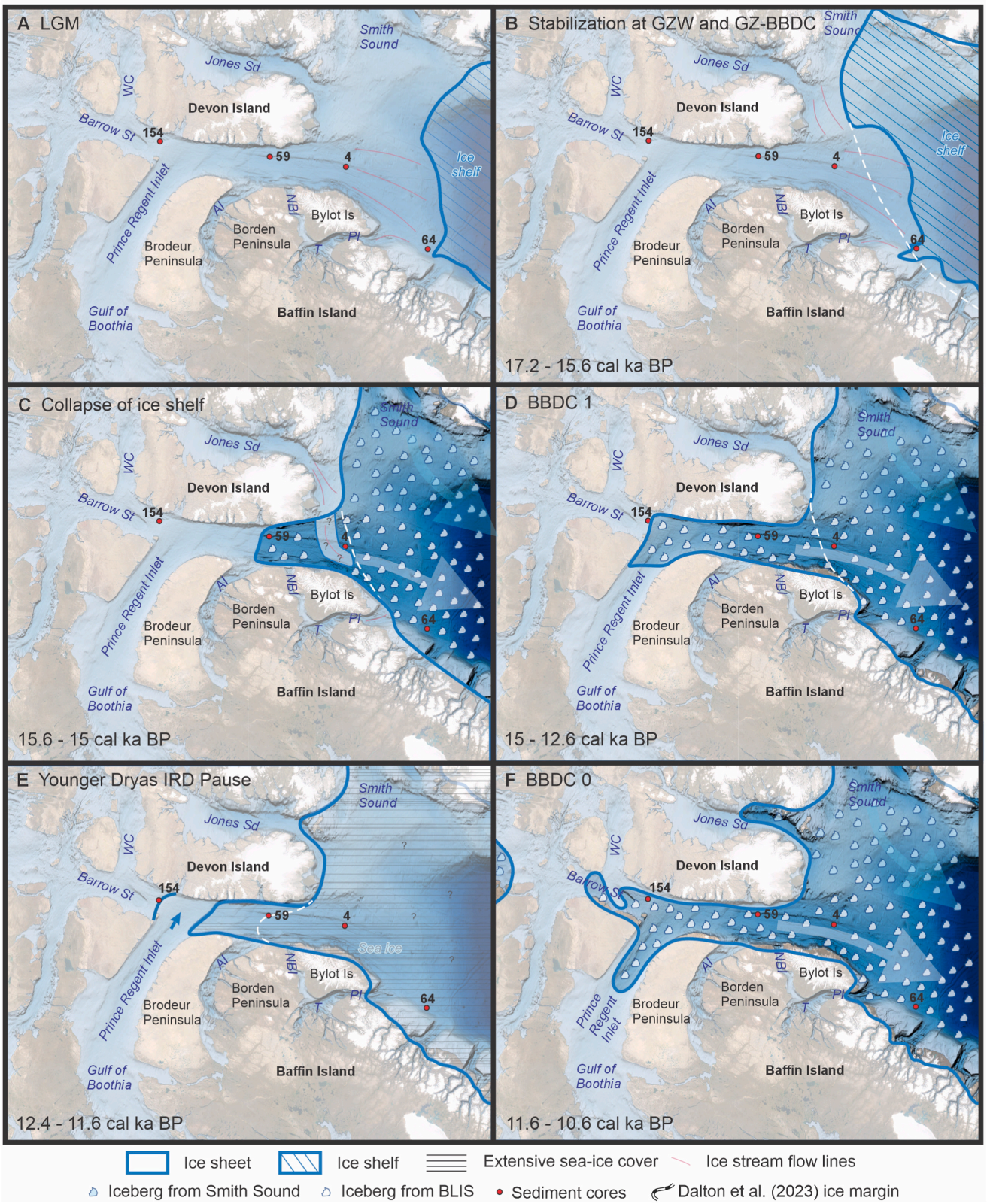

Fig. 8. Series of schematic maps illustrating six phases of ice retreat of the Boothia-Lancaster ice stream A. LGM configuration with confluent BLIS and TIS; B. Stabilization at the large GZW of confluent ice streams after retreat from LGM maximum; C. Collapse of the ice shelf and onset of ice retreat into Lancaster Sound and Pond Inlet; note hypothesized readvance of Jones Sound ice; D. Continued calving margin retreat onto Paleozoic carbonate bedrock in Lancaster Sound responsible for deposition of BBDC 1 and continued retreat into Prince Regent Inlet; E. Readvance of BLIS across Lancaster Sound to southern Devon Island that we correlate to the IRD pause between BBDC 1 and 0; F. Onset of BBDC 0 with ice margin retreat from Devon Island and onward toward the Gulf of Boothia. WC = Wellington Channel; AI = Admiralty Inlet; PI = Pond Inlet; T = Tasiujaq; NBI = Navy Board Inlet.

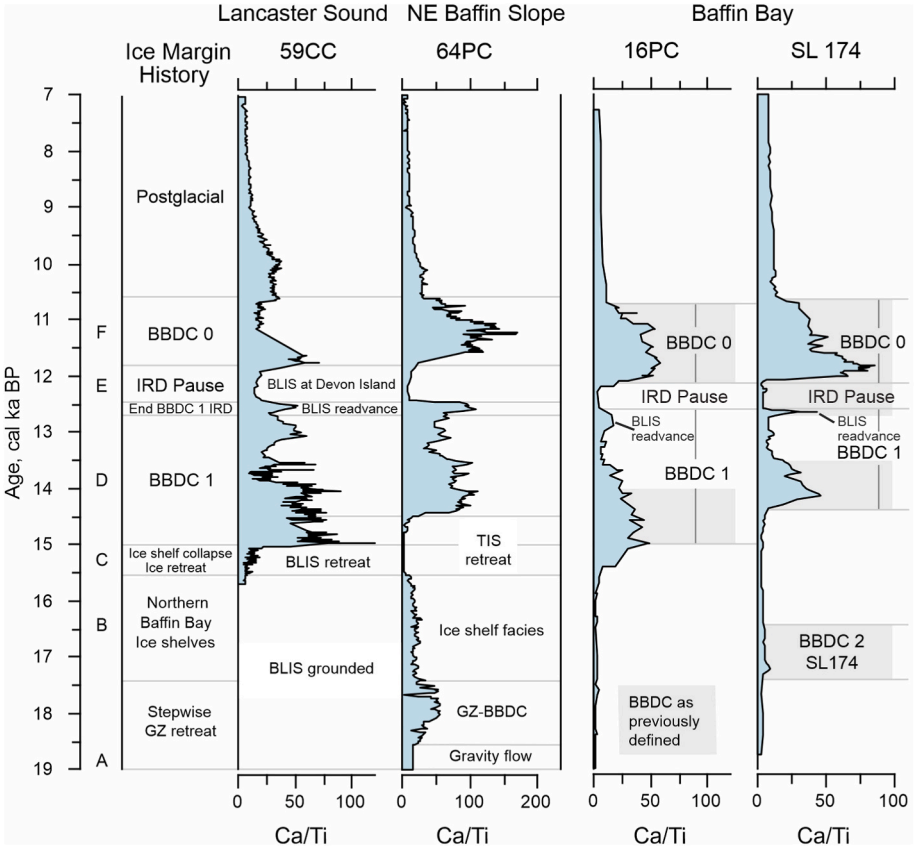

Fig. 9. Comparison of Ca/Ti time series in 59CC and 64 PC and their ice margin history as shown in Fig. 8, against BBDC events in cores 2008029-16 PC from Simon et al. (2012, 2014, 2016) with ages from Simon et al. (2016) and SL 174 (Jackson, 2023; Jackson et al., 2023). The gray boxes represent previously interpreted limits of BBDC events and vertical lines represent the suggested revision of BBDC 1 and 0.

deposit are considered to be LGM age, linear extrapolation of the age model in 64 PC provides a poorly constrained age estimate for the onset and end of GZ-BBDC of ca. 18.5 - ca. 17.2 cal ka BP (Figs. 3 and 8A). We hypothesize that initial retreat of the large BLIS, and confluent TIS, from their maximum grounded extent on the upper slope would produce a distinct IRD unit in more distal localities in Baffin Bay. We also consider that delivery and deposition of IRD at distal sites would have been hindered if the BLIS was fronted by an ice shelf, limiting the flux of debris-bearing icebergs during retreat. However, given the stepped nature of the retreat moraines associated with deposition of GZ-BBDC, there are multiple potential small retreat phases that could produce debris-bearing icebergs and deposit a BBDC event in Baffin Bay. Two axial Baffin Bay sediment cores have dated glaciomarine BBDC events which may be correlative to 64 PC GZ-BBDC: 2008029-16 PC (16 PC) (Simon et al., 2012, 2014, 2016) and GeoTü SL 174 (SL 174) (Jackson et al., 2017, 2023) (Fig. 1). BBDC 2 and 3 of 16 PC are dated to 21 cal ka BP and 23.5–25.5 cal ka BP, respectively (Simon et al., 2016). BBDC 2 and BBDC 3 of SL 174 are dated to 16.4–17.4 cal ka BP and 25.5–26.5 cal ka BP, respectively. All of these BBDC layers are thin (<20 cm) and are emplaced within finer mud intervals lacking significant IRD, suggesting that they record short lived BBDC events preceded and followed by the absence of ice-berg rafting from the BLIS. If we combine the LGM-aged BBDCs (BBDC 3 in SL 174 and BBDC 2 and 3 in 16 PC), they span ca.21–26 cal ka BP. If GZ-BBDC in 64 PC could be proven to match any of these events, that would provide good evidence that GZ-BBDC in 64 PC is an LGM ice-marginal unit produced during release of debris-laden icebergs as BLIS retreated episodically to form the series of retreat moraines (Fig. 2B). Alternatively, we might expect GZ-BBDC in 64 PC to match the deglacial age interval of BBDC 2 in SL 174 of 16.4–17.4 cal ka BP. However, as core 16 PC, which lies upstream of SL-174, does not record a time equivalent BBDC event in the deglacial interval, we suggest that BBDC 2 in SL 174 is an unlikely match for GZ-BBDC and that it may not be derived from the BLIS. Currently there is insufficient evidence to confirm or deny that BBDC events 2 and 3 of Simon et al. (2012, 2014, 2016) and BBDC 3 of Jackson et al. (2017, 2023) are the offshore equivalents of the subglacial/ice marginal GZ-BBDC in 64 PC. However, we think that one of these BBDC events is a likely match.

4.2. GZW and ice shelf of confluent TIS and BLIS

GZ-BBDC transitions upward into the laminated ice shelf facies (L2) (Figs. 3 and 7A). Linear extrapolation of the age model estimates this ice shelf facies was deposited between ca. 17.2 - ca.15.6 cal ka BP and its mineralogy indicates that it comprises sediment suspended in meltwater plumes from both BLIS and TIS. The southward orientation of the TIS GZW (Fig. 2A and B) suggests that the laminated facies was deposited in the sub ice-shelf cavity when the ice streams were confluent (Fig. 2B and 8B). An implication of ice-shelf facies formation early in the deglaciation is that it indicates ice margin stabilization beyond the mouth of Lancaster Sound, on a large grounding zone wedge that can be traced from offshore Pond Inlet to the east of Devon Island (Fig. 2A). This grounding zone wedge is 30–40 km inland from the LGM grounding line identified by Li et al. (2011) and Brouard and Lajeunesse (2017) and consists of TIS and BLIS sediment which merge to create one large landform (Fig. 2B).

4.3. Collapse of the Tasiajuq/Lancaster ice shelf, TIS Retreat into Pond Inlet and BLIS retreat into Lancaster Sound

The black diamicton overlying the laminated ice-shelf facies signals collapse of the ice shelf and retreat of the TIS estimated at ca.15.6 cal ka

BP. Increased foraminiferal productivity in the uppermost 5 cm of the unit is followed abruptly by the onset of BBDC 1 at 14.5 cal ka BP in 64 PC (Fig. 7A). Meanwhile in Lancaster Sound, the ice margin had retreated from the site of 59CC by ca.15.3 cal ka BP, commencing glaciomarine sedimentation (Fig. 7B). The foraminiferal assemblage that provided the date of 15.3, only 5 cm below the contact with BBDC 1, contains abundant, well-preserved *E. clavatum*, which is inconsistent with an ice shelf fronting the retreating ice margin at least immediately before the onset of BBDC 1 (Fig. 7B). The onset of BBDC 1 in 59 CC is marked by the transition from dark brown diamicton to tan calcareous diamicton at ca 15 cal ka BP, ca.500 years prior to the onset of BBDC 1, in 64 PC, of 14.5 cal ka BP (Fig. 7B and 9).

During the rapid retreat of ice into Lancaster Sound, the debutressing of the Lancaster trough likely led to short-lived advances of ice from side valleys into Lancaster Sound. Faint lineations on the seafloor of Lancaster Sound, south of Jones Sound (Fig. 2E; 8C), appear to be overriding Lancaster Sound MSGLs and could provide evidence for advance of ice from Devon Island or Jones Sound into Lancaster Sound shortly after the BLIS retreat. However, apart from these younger, faint, south-flowing lineations on the seafloor of Lancaster Sound at that location, we do not have any further constraints for the timing of the ice advance. Nonetheless, this possible readvance could be responsible for the compacted nature of the basal calcareous diamicton observed in nearby core GeoB22336-4 (Okuma et al., 2023). This unit has a radiocarbon age consistent with deposition during BBDC 1, but it cannot be a subglacial deposit of the BLIS because it was deposited after the BLIS had retreated 150 km NW of GeoB22336-4 by 15.3 cal ka BP (Fig. 8C).

4.4. BBDC 1- BLIS retreat into Prince Regent Inlet

4.4.1. Lack of synchrony in the onset of BBDC 1

Over its full distribution throughout Baffin Bay, the timing of the onset of BBDC 1 varies between 15 and 14.1 cal ka BP (Jackson et al., 2023). We argue that the timing of the onset of BBDC 1 in 59 PC, in Lancaster Sound, is definitive because it is the grounding line retreat of the BLIS off of the Cretaceous and younger bedrock and onto the Paleozoic carbonate bedrock, which is closely dated in this core, that marks initiation of the event (Figs. 8C and 9). As shown by the stratified very dark brown glaciomarine diamicton underlying BBDC 1, the ice margin was already retreating in Lancaster Sound prior to BBDC 1. Ca/Ti values rise slightly below the onset, consistent with the presence of tan calcareous mud blobs, interpreted as till pellets, in the upper part of the dark brown stratified diamicton (Fig. 3; 7B), but the overlying transition to tan calcareous pebbly mud of BBDC 1 marks the base of this marker bed in Baffin Bay. Simon et al. (2012, 2014, 2016) also report the onset of BBDC 1 in Baffin Bay axial core 16 PC at 15 cal ka BP (Fig. 9). Simon et al. (2012) chose the onset of BBDC 1 as the initial peak in Ca/Ti. However, similar to pXRF data in 59 PC, there is a slight rise in Ca/Ti values below the 15 ka BP peak hinting that this core also records the preceding period of BLIS retreat (Fig. 9).

In 64 PC BBDC 1 begins at 14.5 cal ka BP (Kelleher et al., 2022) and 550 km farther south, along the Baffin Island margin, its onset is recorded at 14.4 cal ka BP in SL 174 (Jackson et al., 2023), making the onset of BBDC 1 in these two cores essentially synchronous (Fig. 9). The lack of foraminifera until the upper 5 cm of the black diamicton in 64 PC indicates severe sea-surface conditions possibly associated with siqussaq formed by the abundant icebergs released by the retreating TIS prior to BBDC 1. The upper 5 cm of the black diamicton contains foraminifera dominated by *S. arctica* suggesting severe sea-ice conditions immediately before the onset of BBDC 1 that may have obstructed the detrital carbonate bearing icebergs from tracking over the site of 64 PC (Fig. 7A). Thus, variations in local conditions can explain delayed onset of BBDC 1 in 64 PC and likely in the other cores along the Baffin Island margin.

4.4.2. Updated timing of the end of BBDC 1 in Baffin Bay

Discrepancies in the age of the end of BBDC 1, in Baffin Bay, were summarized by Jackson et al. (2023), with estimates from different studies ranging between 13.5 and 12.8 cal ka BP. As indicated by Jenner et al. (2018) and Kelleher et al. (2022), the top of BBDC 1 is obvious in 64 PC (Figs. 3, 7A and 9). Based on the revised age-depth model (Fig. 3), the end of BBDC 1 is now demonstrated to be younger, 12.4 cal ka BP (12.1–12.9 cal ka BP at 2 σ) (Fig. 3; 7A, 9). The new age model for 59CC allows the top of BBDC 1 to be identified in Lancaster Sound, and this provides the context for understanding why a much earlier end of BBDC 1 has been identified in the more distal axial cores, 16 PC and SL 174 (Fig. 9). Declining sedimentation rates in BBDC 1 are shown by age models in 59CC and 64 PC beginning at ca. 13.6 and 13.4 cal ka BP, respectively (Fig. 3). The lower sedimentation rate is manifested by varied sediment sources (Kelleher et al., 2022) associated with color banding and the three mud layers (Fig. 3), foraminifera increasing in abundance, foraminiferal assemblages shifting away from ice proximal species such as *E. clavatum* in 59CC (Fig. 7B) and *G. oculus* in 64 PC (Fig. 4) and reduced and more variable Paleozoic carbonate input as shown by Ca/Ti values (Figs. 3, 7 and 9). Taken together, these observations indicate reduced glacial sediment input.

In the two dated axial Baffin Bay cores, 16 PC and SL 174, BBDC 1 was previously suggested to end ca. 14 cal ka BP and 13.5 cal ka BP (Fig. 9), coinciding rather well with reduced sedimentation rate and carbonate input from Lancaster Sound during the second half of BBDC 1. However, as is clearly shown in 64 PC, BBDC 1 extends to 12.4 cal ka BP and the new dates on 59CC support this timing as well, suggesting that the distal axial cores 16 PC and SL 174 prominently record the earlier part of BBDC 1, while the younger part is muted (Fig. 9).

4.5. BLIS readvance across Lancaster Sound to Devon Island

Based upon the comparison of Ca/Ti values in the four cores, we suggest an alternative age for the top of BBDC 1 (Fig. 9). We argue that a spike in Ca/Ti values between 12.4 and 12.6 cal ka BP (2 σ range of 12.1–13 cal ka BP) in 59CC and 64 PC is present and correlative to axial Baffin Bay cores 16 PC and SL 174 (Figs. 1 and 9) and that it marks calving of the BLIS as it readvanced out of Prince Regent Inlet across Lancaster Sound to Devon Island (Fig. 8D to E) (MacLean et al., 2017) and formed and/or re-occupied a large grounding zone wedge. By this reasoning, the end of BBDC 1 is defined by a Ca/Ti peak throughout much of Baffin Bay (Fig. 9) and marks the subsequent initiation of a pause in delivery of IRD and detrital carbonate from Lancaster Sound. Unlike the other BBDC intervals, the 12.4 to 12.6 calcareous IRD spike marks an ice advance across deep water with associated calving rather than ice retreat. The fact that this peak marking the end of BBDC 1 is well defined throughout Baffin Bay and within Home Bay (Simon et al., 2014; Jenner et al., 2018; Jackson et al., 2023) demonstrates the strong influence that the BLIS had throughout Baffin Bay, and supports the idea of a rather long pause in both IRD and carbonate delivery from Lancaster Sound between BBDC 1 and BBDC 0 (Fig. 9).

4.6. Stabilization of BLIS at Devon Island and formation of the muddy pause in IRD

The correlative mud layers in 59CC and 64 PC mark a significant reduction in sedimentation rate and glacial input between BBDC 1 and BBDC 0 lasting from 12.4 to 11.6 cal ka BP (Figs. 3 and 7). The reduced sedimentation rate could be considered the culmination of the slowing sedimentation rate that began ca. 13.6 (59CC) and 13.4 (64 PC) cal ka BP (Fig. 3). The pause in iceberg rafting reflects stabilization of the ice margin in Lancaster Sound. We suggest that stabilization of the BLIS on Devon Island reduced calving and mass loss, for the duration of the muddy pause in IRD. However, the configuration of the ice margin facing Lancaster Sound is unknown. The relative lack of IRD during the muddy pause suggests it may have been buttressed by an ice shelf and/or heavy sea ice (Fig. 8E). Age control on core 154 in Barrow Strait (Fig. 8) indicates that the BLIS had retreated prior to 11.5 cal ka BP (Pieńkowski

et al., 2014; MacLean et al., 2017) which is consistent with the timing of the onset of BBDC 0 at 11.6 cal ka BP (Fig. 8F).

The foraminiferal faunas in the IRD pause mud layer are similar in both cores and reflect a stratified water column with chilled Atlantic Water and a glacial meltwater lid on which sea-ice cover formed (Figs. 4 and 7). The mud layer is bioturbated in both cores, most noticeably at the base where the darker mud is worked downward 1 cm into the underlying tan calcareous mud, reflecting significant, slowing of sedimentation. This IRD pause reflects low calving rates and higher stability in other ice margins terminating in Lancaster Sound, and suggests that Younger Dryas cooling and pervasive sea ice, as indicated by the foraminiferal faunas, may have stabilized ice margins throughout the region, even with the presence of chilled Atlantic Water at the seabed as indicated by abundant *C. neoteretis* (Figs. 4 and 7). The age models show that the muddy pause in ice rafting started after the beginning of the Younger Dryas cool period and ended during the earliest Holocene with deposition of BBDC 0, marking the resumption of iceberg rafting during the BLIS retreat back into Prince Regent Inlet (Fig. 8F) and toward the Gulf of Boothia by 10 cal ka BP (Hooper, 1996; MacLean et al., 2017; Tremblay and Lamothe, 2022).

4.7. BBDC 0: 11.6–10.6 cal ka BP

We attribute the onset of BBDC 0, ca 11.6 cal ka BP, to the southward retreat of the BLIS into Prince Regent Inlet from its Younger Dryas margin in western Lancaster Sound (Fig. 8F). Previous studies have placed BBDC 0 within the Younger Dryas cold period (Jackson et al., 2023; Simon et al., 2012, 2014; Kelleher et al., 2022). The improved age constraints presented from cores proximal to the BLIS make it clear that the onset of BBDC 0 coincided with warming at the beginning of the Holocene. A major calving event marking destabilization and final retreat of the BLIS is consistent with warming climate. The new correlation of the base of BBDC 0 from cores 59CC and 64 PC to more distal sites in Baffin Bay is complicated by age-depth models of cores 16 PC and SL 174, which place the onset of BBDC 0 closer to ca.12.0 cal ka BP (Simon et al., 2016; Jackson et al., 2023, Fig. 9). This slight deviation in the chronology may result from uncertainties in the radiocarbon ages, and/or additional uncertainties in calibration.

4.8. Lessons from the retreat history of the BLIS

After a long period of stability, the Antarctic ice sheets have begun to lose their buttressing ice shelves and the grounding zones of large outlet glaciers, such as Thwaites Glacier, are showing signs of destabilizing; these changes are leading to increasing concern about tipping points and rapid sea-level rise (cf. Scambos et al., 2017; Fricker et al., 2025). Although an imperfect analogue, the full retreat history of the BLIS presented herein, demonstrates the role of ice shelves in modulating the dynamics of ice stream retreat and in governing the modes and rates of glaciomarine sedimentation in both ice-proximal and -distal environments that have applications to modern ice sheet instabilities and mass balance changes (cf. DeConto et al., 2021).

The timing of initial stepwise ice retreat of the BLIS/TIS from the LGM position (Fig. 8A and B) is not well documented, but LGM and younger BBDC events in axial cores from Baffin Bay provide targets for potential correlations to initial retreat from the LGM that formed GZ-BBDC and the underlying gravity flow deposit. If we tentatively postulate that this initial retreat is correlative with BBDC 2 (21 cal ka BP) and/or BBDC 3 (23.5–25 cal ka BP) of Simon et al. (2016), then the BLIS ice margin retreated from its maximum position ca.350 km to the site of 59CC by 15.3 cal ka BP within ca.10 kyr (Fig. 8A–C). Within this 10 kyr timeframe was also a period of stability as reflected by the large grounding zone wedge and deposition of the laminated ice-shelf facies in 64 PC (Fig. 8B), a manifestation of a northern Baffin Bay ice shelf (Couette et al., 2022).

The age model in 64 PC does not adequately predict the beginning or end of sub ice-shelf deposition, but other evidence around Baffin Bay provides some potential timing. The Greenland Ice Sheet lost its fringing ice shelf off central West Greenland between 17 and 16 cal ka BP (Jennings et al., 2017, 2018) and glacial isostatic adjustment (GIA) modeling has suggested that the maximum ice extent off West Greenland was achieved ca. 16.5 ka, with retreat underway by 16 ka (Lecavalier et al., 2014). Jackson et al. (2023) dated a BBDC 2 in core SL 174 (Fig. 1) at 16.4–17.4 cal ka BP and showed that it matches the timing of H1 in NW Labrador Sea core 97048-07 (Rashid et al., 2019), indicating that ice sheet instabilities were widespread at this time. This timing also coincides with the initial acceleration of global sea level rise ca. 17 cal ka BP (Stanford et al., 2011) which could have been a driver of retreat along with subsurface penetration of warm Atlantic Water (Jennings et al., 2017). However, the effect of global sea level rise may have been offset by glacioisostatic rebound as ice load was removed by deglaciation.

At the onset of BBDC 1, ca. 15 cal ka BP (Fig. 8D), the ice margin was retreating westward within Lancaster Sound and after an unknown period of stability at the GZWs west of 59CC (Fig. 2A), it continued its westward and southward retreat into Prince Regent Inlet (equating to ca.200 km in 2.5 kyr) (Fig. 8D), presumably releasing a large volume of freshwater and sediment in meltwater and icebergs. This release was especially rapid between 15 and ca. 13.5 cal ka when the sedimentation rates and release of detrital carbonate-charged icebergs was greatest (Fig. 3). The timing of this period of major ice retreat coincides with coastal ice retreat in the Clyde Foreland, Baffin Island at ca 15 ka BP based on cosmogenic exposure ages (Briner et al., 2005) and with the onset of rapid sedimentation in Baffin Bay (Okuma et al., 2024). It also coincides with meltwater pulse (Mwp) 1a, ca. 14.3–12.8 cal ka BP, when rates of sea-level rise are estimated to have exceeded 1 m/century (Stanford et al., 2011), with the highest rates occurring between ca.13.3 and 14.3 cal ka BP (Stanford et al., 2011). The pause in IRD between BBDC 1 and 0 in the Younger Dryas cool period, from 12.4 to 11.6 cal ka

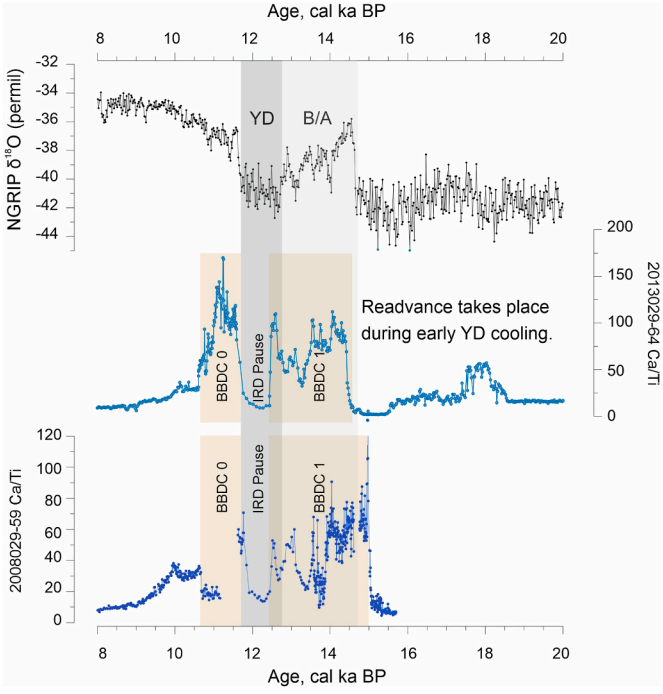

Fig. 10. Ca/Ti vs age in 59CC and 64 PC compared with $\delta^{18}O$ data from the North GRIP ice core (NGRIP community members, 2004; Rasmussen et al., 2006), illustrating the timing of BBDC 1 synchronous with the Bølling-Allerød (B/A), the IRD pause synchronous with the Younger Dryas (YD), and BBDC 0 beginning after the end of the Younger Dryas chronozone, in the early Holocene.

BP (Fig. 8E), matches well with the timing of the break between Mwp 1a and Mwp 1b (Fig. 10). Mwp 1b began at 11.5 cal ka BP and extended into the Holocene (Stanford et al., 2011). The onset of Mwp 1b very closely coincides with the beginning of BBDC 0 as the BLIS retreated into Prince Regent Inlet and further south (Tremblay and Lamothe, 2022). Although we do not know the quantitative contribution of the retreating BLIS to global mean sea level rise, during Mwp 1a and 1b, it clearly was a contributor, along with other ice sheets and ice margins that were similarly responding to climate warming (Vaughan et al., 2024; Coonin et al., 2025).

4.9. Climatic significance of the IRD pause between BBDC 1 and 0 in Baffin Bay?

Our current core data are insufficient to test whether the IRD pause between BBDC 1 and 0 has a climatic component or whether the readvance to a pinning point is related instead to ice stream dynamics alone. Distribution of icebergs containing debris and meltwater plumes is partly dictated by sea-ice cover, ice shelves, ocean circulation and the rate of iceberg melt. If the IRD pause between BBDC 1 and 0 reflects Younger Dryas cooling involving stabilization of ice sheet outlets draining into Lancaster Sound, one might expect to observe similar conditions on the West Greenland margin. Several studies have associated large GZWs in large West Greenland cross-shelf troughs with ice margin stabilization or even readvance inferred or hypothesized to be in response to Younger Dryas cooling (Ó Cofaigh et al., 2013; Sheldon et al., 2016; Hogan et al., 2016; Newton et al., 2017). Although BBDC 1 and 0 have been observed in many areas of Baffin Bay, including on the central West Greenland upper slope and shelf (Jennings et al., 2014, 2017; Sheldon et al., 2016; Jackson et al., 2017), southwestern Baffin Bay and Home Bay (Jenner et al., 2018), these events are understandably less pronounced being more distal to the Lancaster Sound source. Other than the onset of BBDC 1, which has been dated consistently in multiple cores on the Greenland margin and matches temporally to the age of BBDC 1 near to the source, the correlation between BBDC 0 on the Greenland versus Baffin Island side of Baffin Bay is less coherent (cf. Jackson et al., 2017). However, this has not been examined extensively. It will be important in future research to attempt to date the BBDC events and GZW emplacement on the West Greenland margin to better understand the responses of ice sheets to post LGM warming on both sides of Baffin Bay.

5. Summary and conclusions

Combined geomorphological and sediment core data are used to reconstruct the LGM to Holocene history of the BLIS and TIS, resulting in revised timing for the onset and end of BBDC 1 and BBDC 0, which are important stratigraphic markers in Baffin Bay. Facies in 64 PC reflect episodic retreat from ice margins attained during the LGM and subsequent establishment of a stable ice-shelf fronted margin that persisted until ca. 17 cal ka BP. Cores 64 PC and 59CC indicate that after the ice shelf collapsed, the confluent ice streams separated and retreated into Lancaster Sound and Pond Inlet. In both cores, BBDC 1 records a period of significant ice stream retreat sustained by high calving rates, during which the BLIS retreated into Prince Regent Inlet. Termination of BBDC 1 coincided with a readvance of the BLIS to Devon Island. The age of BBDC 1 is here revised from earlier studies to ca. 15–12.4 cal ka BP. The pause in IRD deposition between BBDC 1 and BBDC 0 reflects a significant reduction in calving from the BLIS margin, which is interpreted to have stabilized at Devon Island during the Younger Dryas chronozone. The cause of the ice readvance is unknown. It could reflect a response to cooling, or it could reflect reorganization of ice flow not directly related to climatic cooling (MacLean et al., 2017). Resumption of significant ice-rafting, resulting in deposition of BBDC 0 from 11.6 to 10.6 cal ka BP, marks retreat of the BLIS back into Prince Regent Inlet and southward toward Gulf of Boothia, ending with the opening of Parry Channel to throughflow between the Arctic Ocean and Baffin Bay (Kelleher et al., 2022). Our new reconstruction of the dynamics of the BLIS highlights an earlier retreat into Lancaster Sound than previous studies have suggested. Our deglaciation isochrones differ markedly from those portrayed in (Dalton et al., 2023) which appear to have been based on radiocarbon dates constraining the age of the marine limit on the south coast of Devon Island (Dyke, 1999). We suggest, however, that the age of the marine limit along the south coast of Devon Island was primarily controlled by the dynamics of the deglacial Devon Island Ice Cap which advanced into Lancaster Sound following the retreat of the BLIS.

CRediT authorship contribution statement

Anne Jennings: Conceptualization, Formal analysis, Funding acquisition, Investigation, Project administration, Writing – original draft, Writing – review & editing. **Kimberley Jenner:** Conceptualization, Visualization, Writing – original draft, Writing – review & editing. **Alexandre Normandeau:** Conceptualization, Visualization, Writing – original draft. **Wendy Roth:** Resources, Formal analysis, Investigation. **John Andrews:** Formal analysis, Investigation. **Robert Kelleher:** Formal analysis. **Juliette Girard:** Investigation, Formal analysis. **Brendan Reilly:** Investigation, Formal analysis. **Calvin Campbell:** Funding acquisition, Project administration. **Robbie Bennett:** Investigation, Formal analysis.

Declaration of competing interest

The authors declare that they have no known competing financial interests or personal relationships that could have appeared to influence the work reported in this paper.

Acknowledgements

This work was funded by the United States National Science Foundation, grants NSF OPP-1804504 and NSF-OCE-2112547 and the Natural Hazards and Climate Change Geoscience Program of the Geological Survey of Canada. We thank Kate Jarrett, GSC Atlantic, for providing samples and access to data and the GSC core repository. Jenna Higgins collected the pXRF data for 59 PC and 64 PC. We thank Thomas Lakeman and an anonymous reviewer for their helpful comments and suggestions to improve this manuscript.

Data availability statement

Data generated from this study will be archived in the GSC Atlantic Expedition database. The core data are archived at and the US Arctic Data Centerhttps://arcticdata.io

References

Aksu, A.E., 1981. Late Quaternary Stratigraphy, Paleoenvironmentology, and Sedimentation History of Baffin Bay and Davis Strait. Dalhousie University, Halifax, NS, p. 771. PhD Thesis.

Aksu, A.E., Piper, D.J.W., 1987. Late quaternary sedimentation in Baffin Bay. Can. J. Earth Sci. 24, 1833–1846.

Alley, R.B., Clark, P.U., Huybrechts, P., Joughin, I., 2005. Ice-sheet and sea-level changes. Science 310, 456–460. https://doi.org/10.1126/science.1114613.

Andrews, J.T., Kirby, M.E., Aksu, A., Barber, D.C., Meese, D., 1998. Late Quaternary detrital carbonate events in Baffin Bay (671–741N): do they correlate with and contribute to Heinrich events in the North Atlantic? Quat. Sci. Rev. 17, 1125–1137.

Andrews, J.T., Jenner, K.A., Campbell, C.D., 2020. Linking marine core lithofacies and mineral and grain-size compositions on the Baffin Island margin: changes in provenance and transport. J. Sediment. Res. 90, 1–13. https://doi.org/10.2110/jsr.2020.50.

Andrews, J.T., Piper, D.J.W., Jennings, A.E., Miller, G.H., 2024. Growth of the Laurentide and Innuitian ice sheets during MIS 5 recorded in distal marine sediment. Quat. Sci. Rev. 328, 108532. https://doi.org/10.1016/j.quascirev.2024.108532.

Batchelor, C.L., Christie, F.D.W., Ottesen, D., et al., 2023. Rapid, buoyancy-driven ice-sheet retreat of hundreds of metres per day. Nature 617, 105–110. https://doi.org/10.1038/s41586-023-05876-1, 2023.

Batchelor, C.L., Dowdeswell, J.A., 2015. Ice-sheet grounding-zone wedges (GZWs) on high-latitude continental margins. Mar. Geol. 363, 65–92. https://doi.org/10.1016/j.margeo.2015.02.001.

Batchelor, C.L., Krawczyk, D.W., O'Brien, E., et al., 2024. Shelf-break glaciation and an extensive ice shelf beyond northwest Greenland at the Last Glacial Maximum. Mar. Geol. https://doi.org/10.1016/j.margeo.2024.107375.

Bennett, R., Campbell, D.C., Furze, M.F.A., 2013. The shallow stratigraphy and geohazards of the northern Baffin Island shelf: studies to 2012. Geological Survey of Canada, Open File 7355, 42.

Bennett, R., Campbell, D.C., Furze, M.F.A., Haggart, J.W., 2014. The shallow stratigraphy and geohazards of the NE Baffin shelf and lancaster Sound. Bull. Can. Petrol. Geol. 62 (4), 217–231. https://doi.org/10.2113/gscpgbull.62.4.217.

Bennett, R., Maclean, B., Blasco, S., Hughes-Clarke, J., 2016. Glacial lineations in Navy board inlet, Nunavut, Canada. Geological Society, London, Memoirs 46, 49–50. https://doi.org/10.1144/M46.56.

Blaauw, M., Christen, J.A., 2011. Flexible paleoclimate age–depth models using an autoregressive gamma process. Bayesian Analysis 6, 457–474. https://doi.org/10.1214/ba/1339616472.

Briner, J.P., Miller, G.H., Davis, P.T., Finkel, R., 2005. Cosmogenic exposure dating in arctic glacial landscapes: implications for the glacial history of northeastern Baffin Island, Arctic Canada. Can. J. Earth Sci. 42, 67–84. https://doi.org/10.1139/e04-102.

Brouard, E., Lajeunesse, P., 2017. Maximum extent and decay of the Laurentide ice sheet in western Baffin Bay during the last glacial episode. Sci. Rep. 7, 10711. https://doi.org/10.1038/s41598-017-11010-9.

Campbell, D.C., 2014. CCGS Hudson expedition 2013-029 geological hazard assessment of Baffin Bay and biodiversity assessment of Hatton basin, august 14-september 16, 2013. Geological Survey of Canada, Open file 7594, 124. https://doi.org/10.4095/293694.

Campbell, C., de Vernal, A., 2009. Marine geology and paleoceanography of Baffin Bay and adjacent areas nain, NL to Halifax, NS august 28-september 23, 2008. Geological Survey of Canada Open file 5989, 212. https://doi.org/10.4095/261330.

Campbell, D.C., Jenner, K.A., Higgins, J., Piper, D.J.W., 2017. Analysis of piston cores and high-resolution sub-bottom profiler data, Baffin Bay slope, Nunavut. Geological Survey of Canada, Open File 8135, 179. https://doi.org/10.4095/300835.

Clark, P.U., 1987. Subglacial sediment dispersal and till composition. J. Geol. 95, 527–541.

Coonin, A.N., Lau, H.C.P., Coulson, S., 2025. Meltwater Pulse 1A sea-level-rise patterns explained by global cascade of ice loss. Nat. Geosci. 18, 254–259. https://doi.org/10.1038/s41561-025-01648-w.

Couette, P.O., Lajeunesse, P., Ghienne, J.F., Dorschel, B., Gebhardt, C., Hebbeln, D., Brouard, E., 2022. Evidence for an extensive ice shelf in northern Baffin Bay during the last glacial maximum. Commun. Earth Environ. 3, 225. https://doi.org/10.1038/s43247-022-00559-7.

Currie, L., Brent, T., Turner, E., 2020. Offshore bedrock geology of Eclipse Sound and Pond inlet: connecting the structure and stratigraphy of Bylot and northern Baffin islands. Can. J. Earth Sci. 57, 1254–1267. https://doi.org/10.1139/cjes-2019-0159.

Dalton, A.S., Dulfer, H.E., Margold, M., Heyman, J., Clague, J.J., Froese, D., Gauthier, M. S., Hughes, A.L.C., Jennings, C.E., Norris, S.L., Stoker, B.J., 2023. Deglaciation of the north American ice sheet complex in calendar years based on a comprehensive database of chronological data: NADI-1. Quat. Sci. Rev. 321 (2023). https://doi.org/10.1016/j.quascirev.2023.108345. Article 108345.

Dalton, A.S., Margold, M., Dulfer, H., Norris, S.L., Tarasov, L., 2024. Response of North American ice sheets to the Younger Dryas cold reversal (12.9 to 11.7 ka). Earth Sci. Rev. 255, 104845. https://doi.org/10.1016/j.earscirev.2024.104845.

Dalton, A.S., Margold, M., Stokes, C.R., Tarasov, L., Dyke, A.S., Adams, R.S., et al., 2020. An updated radiocarbon-based ice margin chronology for the last deglaciation of the North American Ice Sheet Complex. Quat. Sci. Rev. 234, 106223. https://doi.org/10.1016/j.quascirev.2020.106223.

DeConto, Robert M., Pollard, David, Alley, Richard B., Velicogna, Isabella, Gasson, Edward, Gomez, Natalya, Sadai, Shaina, Condron, Alan, Gilford, Daniel M., Ashe, Erica L., Kopp, Robert E., Li, Dawei, Dutton, Andrea, 2021. The Paris Climate Agreement and future sea-level rise from Antarctica. Nature 593, 83e89. https://doi.org/10.1038/s41586-021-03427-0.

Dreutter, S., Geils, J., Lütjens, M., Köpke, F., Dorschel, B., 2023. Multibeam bathymetry processed data (Kongsberg EM712 entire dataset) of RV MARIA S. MERIAN during cruise MSM66, Baffin Bay, north Atlantic ocean. PANGAEA. https://doi.org/10.1594/PANGAEA.955108.

Dyke, A.S., Andrews, J.T., Clark, P.U., England, J.H., Miller, G.H., Shaw, J., Veillette, J. J., 2002. The Laurentide and Innuitian ice sheet during the last glacial maximum. Quat. Sci. Rev. 21, 9–31. https://doi.org/10.1016/S0277-3791(01)00095-6.

Dyke, Arthur, 1999. Last glacial maximum and deglaciation of Devon island, arctic Canada: support for an Innuitian ice sheet. Quat. Sci. Rev. 18, 393–420.

Dyke, A.S., Hooper, J.M.G., 2001. Deglaciation of northwest Baffin island. Nunavut. Geological Survey of Canada. Map 1999A, scale 1:500 000.

Eberl, D.D., 2003. User Guide to RockJock: A Program for Determining Quantitative Mineralogy from X-Ray Diffraction Data. United States Geological Survey, Washington, DC, p. 40. Open File Report 03-78.

England, J.H., Atkinson, N., Bednarski, J.B., Dyke, A.S., Hodgson, D.A., Ó'Cofaigh, C., 2006. The Innuitian ice sheet: configuration, dynamics and chronology. Quat. Sci. Rev. 25, 689–703. https://doi.org/10.1016/j.quascirev.2005.08.007.

Feyling-Hanssen, R.W., 1976. The Clyde Foreland formation, a micropaleontological study of quaternary stratigraphy. In: 1st International Symposium on Benthonic Foraminifera of Continental Margins, Part B: Paleoecology and Biostratigraphy, vol. 1. Maritime Sediments Special Publication, pp. 315–377.

Fricker, H.A., Galton-Fenzi, B.K., Walker, C.C., Freer, B.I.D., Padman, L., DeConto, R., 2025. Antarctica in: drivers of deep uncertainty in projected ice loss. Science 387, 601–609.

Furze, M., Pieńkowski, A., McNeely, M., Bennett, R., Cage, A., 2017. Deglaciation and ice shelf development at the northeast margin of the Laurentide Ice Sheet during the Younger Dryas chronozone. Boreas 47, 271–296. https://doi.org/10.1111/bor.12265.

GEBCO Compilation Group, 2024. GEBCO 2024 Grid. https://doi.org/10.5285/1c44ce99-0a0d-5f4f-e063-7086abc0ea0f.

Harrison, J., Brent, T., Oakey, G., 2011a. Chapter 40: Baffin Fan and its inverted rift system of Arctic eastern Canada: stratigraphy, tectonics and petroleum resource potential. Geological Society 35, 595–626. https://doi.org/10.1144/M35.40. London, Memoirs.

Harrison, J.C., St-Onge, M.R., Petrov, O.V., Strelnikov, S.I., Lopatin, B.G., Wilson, F.H., Tella, S., Paul, D., Lynds, T.L., Shokalsky, S.P., Hults, C.K., Bergman, S., Jepsen, H.F., Solli, A., 2011b. Geological Map of the Arctic. Geological Survey of Canada. https://doi.org/10.4095/287868. A" Series Map, 2159A.

He, F., Clark, P.U., 2022. Freshwater forcing of the Atlantic meridional overturning circulation revisited. Nat. Clim. Change 12, 449–454. https://doi.org/10.1038/s41558-022-01328-2.

Heaton, T., Köhler, P., Butzin, M., Bard, E., Reimer, R., Austin, W., Skinner, L., 2020. Marine20—the marine radiocarbon age calibration curve (0–55,000 cal BP). Radiocarbon 62 (4), 779–820. https://doi.org/10.1017/RDC.2020.68.

Hiscott, R.N., Aksu, A.E., Nielsen, O.B., 1989. Provenance and dispersal patterns, pliocene - Pleistocene section at site 645, Baffin Bay. Proc. ODP, Sci. Results 105, 31–52.

Hogan, K.A., Jakobsson, M., Mayer, L., Reilly, B.T., Jennings, A.E., Stoner, J.S., Nielsen, T., Andresen, K.J., Nørmark, E., Heirman, K.A., Kamla, E., Jerram, K., Stranne, C., Mix, A., 2020. Glacial sedimentation, fluxes and erosion rates associated with ice retreat in Petermann Fjord and Nares Strait, north-west Greenland. Cryosphere 14, 261e286. https://doi.org/10.5194/tc-14-261-2020.

Hogan, K.A., Ó Cofaigh, C., Jennings, A., Dowdeswell, J., Hiemstra, J., 2016. Deglaciation of a major palaeo-ice stream in disko trough, west Greenland. Quat. Sci. Rev. 147, 5–26. https://doi.org/10.1016/j.quascirev.2016.01.018.

Hooper, M.J.G., 1996. Glacial history and Holocene sea level regression in the Foxe/Baffin sector of the Laurentide ice sheet, northwest Baffin island, arctic Canada. PhD Thesis. Department of Earth and Planetary Sciences. University of Alberta, Edmonton, Alberta, p. 282.

Jackson, G.D., 2000. Geology of the Clyde-Cockburn Land Map Area, North-Central Baffin Island, Nunavut, vol. 440. Geological Survey of Canada, Memoir, p. 303.

Jackson, R., Carlson, A., Hillaire-Marcel, C., Wacker, L., Vogt, C., Kucera, M., 2017. Asynchronous instability of the North American-Arctic and Greenland ice sheets during the last deglaciation. Quat. Sci. Rev. https://doi.org/10.1016/j.quascirev.2017.03.020.

Jackson, R., 2023. Data from Marine Sediment Core GeoTü SL 174. GEUS Dataverse, p. V1. https://doi.org/10.22008/FK2/Q0CNLI (Baffin Bay).

Jackson, R., Frederichs, T., Schulz, H., Kucera, M., 2023. Chronology of detrital carbonate events in Baffin Bay reveals different timing but similar average recurrence time of North American-Arctic and Laurentide ice sheet collapse events during MIS 3. Earth Planet Sci. Lett. 613, 118191. https://doi.org/10.22008/FK2/Q0CNLI.

Jenner, K.A., Campbell, D., Piper, D., 2018. Along-slope variations in sediment lithofacies and depositional processes since the Last Glacial Maximum on the northeast Baffin margin, Canada. Mar. Geol. 405, 92–107. https://doi.org/10.1016/j.margeo.2018.07.012.

Jennings, A.E., Andrews, J.T., Ó Cofaigh, C., St-Onge, G., Belt, S., Cabedo-Sanz, P., Pearce, C., Hillaire- Marcel, C., Calvin Campbell, D., 2018. Baffin Bay paleoenvironments in the LGM and HS1: resolving the ice-shelf question. Mar. Geol. 402, 5–16. https://doi.org/10.1016/j.margeo.2017.09.002.

Jennings, A., Andrews, J., Ó Cofaigh, C., St-Onge, G., Sheldon, C., Belt, S., Cabedo-Sanz, P., Hillaire-Marcel, C., 2017. Ocean forcing of Ice Sheet retreat in central west Greenland from LGM to the early Holocene. Earth Planet Sci. Lett. 472, 1–13. https://doi.org/10.1016/j.epsl.2017.05.007.

Jennings, A., Andrews, J., Reilly, B., Walczak, M., Jakobsson, M., Mix, A., Stoner, J., Nicholls, K., Cheseby, M., 2020a. Modern foraminiferal assemblages in northern Nares Strait, petermann Fjord, and beneath Petermann ice tongue, NW Greenland. Arctic Antarct. Alpine Res. 52, 491–511. https://doi.org/10.1080/15230430.2020.1806986.

Jennings, A.E., Normandeau, A., Jenner, K.A., Andrews, J., Kelleher, R., Marchito, T., Girard, J., Reilly, B., 2025. Northern Baffin Bay Sediment Core Evidence for Boothia-Lancaster Ice Stream Retreat from Last Glacial Maximum Extent and for its Role in the Origin of Baffin Bay Detrital Carbonate (BBDC) Events 0, 1 and 2 (2019-2024). Arctic Data Center. https://doi.org/10.18739/A2KD1QN3M.

Jennings, A.E., Reilly, B., Andrews, J.T., Hogan, K., Walczak, M., Jakobsson, M., Stoner, J., Mix, A., Nicholls, K.W., O'Regan, M., Prins, M.A., Troelstra, S.R., 2022. Modern and early Holocene ice shelf sediment facies from Petermann Fjord and northern Nares Strait, northwest Greenland. Quat. Sci. Rev. 283, 107460. https://doi.org/10.1016/j.quascirev.2022.107460.

Jennings, A.E., Seidenkrantz, M.-S., Knudsen, K.L., 2020b. Glomulina oculus, new calcareous foraminiferal species from the high Arctic: a potential indicator of a nearby marine-terminating glacier. J. Foraminifer. Res. 50 (2), 219–234. https://doi.org/10.2113/gsjfr.52.2.219.

Jennings, A.E., Walton, M.E., Ó Cofaigh, C., Kilfeather, A., Andrews, J.T., Ortiz, J.D., de Vernal, A., Dowdeswell, J.A., 2014. Paleoenvironments during younger Dryas-early Holocene retreat of theGreenland ice sheet from outer Disko trough, central West Greenland. J. Quat. Sci. 29, 27–40. https://doi.org/10.1002/jqs.2652.

Kelleher, R.V., Jennings, A.E., Andrews, J.T., Brooks, N.K.S., Marchitto, T., Feng, S., Woelders, L., Normandeau, A., Jenner, K., Bennett, R., Brookins, S., 2022. Late glacial retreat of the Lancaster Sound ice stream and early Holocene onset of arctic/Atlantic throughflow in the arctic island channels. Arctic Antarct. Alpine Res. 54 (1), 395–427. https://doi.org/10.1080/15230430.2022.2110689.

Klassen, R.A., 1985. An outline of the glacial history of Bylot island, District of Franklin, N.W.T. In: Andrews, J.T. (Ed.), Quaternary Environments, Eastern Canadian Arctic, Baffin Bay and Western Greenland. Allen and Unwin, Boston, p. 428e460.

Klassen, R.A., 1993. Quaternary Geology and Glacial History of Bylot Island, Northwest Territories, vol. 429. Geological Survey of Canada, Memoir, p. 93.

Klassen, R.A., Fisher, D.A., 1988. Basal flow conditions at the northeastern margin of the Laurentide ice sheet, Lancaster Sound. Can. J. Earth Sci. 25, 1740–1750.

Lakeman, T.R., Pieńkowski, A.J., Nixon, F.C., Furze, M.F., Blasco, S., Andrews, J.T., King, E.L., 2018. Collapse of a marine-based ice stream during the early Younger Dryas chronozone, western Canadian Arctic. Geology 46, 211–214. https://doi.org/10.1130/G39665.1.

Lecavalier, B.S., Milne, G.A., Simpson, M.J.R., Wake, L., Huybrechts, P., Tarasov, L., Kjeldsen, K.K., Funder, S., Long, A.J., Woodroffe, S., Dyke, A.S., Larsen, N., 2014. Amodel of Greenland ice sheet deglaciation constrained by observations of relative sea level and ice extent. Quat. Sci. Rev. 102, 54–84. https://doi.org/10.1016/j.quascirev.2014.07.018.

Li, G., Piper, D.J.W., Campbell, D.C., 2011. The quaternary Lancaster Sound trough-mouth fan, NW Baffin Bay. J. Quat. Sci. 26, 511–522. https://doi.org/10.1002/jqs.1479.

MacLean, B., Blasco, S., Bennett, R., Lakeman, T., Pieńkowski, A.J., Furze, M.F.A., Hughes Clarke, J., Patton, E., 2017. Seafloor features delineate late Wisconsinan ice stream configurations in eastern Parry Channel, Canadian arctic Archipelago. Quat. Sci. Rev. 160, 67–84. https://doi.org/10.1016/j.quascirev.2017.02.001.

MacLean, B., Falconer, R.K.H., 1979. Geological-geophysical studies in Baffin Bay and Scott Inlet-Buchan Gulf and Cape Dyer-Cumberland Sound areas of the Baffin island shelf. Curr. Res. Geol. Surv. Can. 79–01B, 231–244.

MacLean, B., Falconer, R.K.H., Clarke, D.B., 1978. Tertiary basalts of western Davis Strait: bedrock core samples and geophysical data. Can. J. Earth Sci. IS, 773–780.

Margold, M., Stokes, C.R., Clark, C.D., 2018. Reconciling records of ice streaming and ice margin retreat to produce a palaeogeographic reconstruction of the deglaciation of the Laurentide Ice Sheet. Quat. Sci. Rev. 189, 1–30. https://doi.org/10.1016/j.quascirev.2018.03.013.

McCuaig, S.J., 1994. Glacial chronology of the south Bylot and Salmon River lowlands, N.W.T., using erratic dispersal patterns, cosmogenic dating, radiocarbon dating and lichenometry. M.Sc.thesis. Carleton University, Ottawa, Unpublished.

McManus, J.F., Francois, R., Gherardi, J.-M, Keigwin, L.D., Brown-Leger, S., 2004. Collapse and rapid resumption of Atlantic meridional circulation linked to deglacial climate changes. Nature 428, 834–837.

Miall, A.D., Balkwill, H.R., Hopkins Jr., W.S., 1980. Cretaceous and Tertiary Sediments of Eclipse Trough, Bylot Island Area, Arctic Canada, and Their Regional Setting. Geological Survey of Canada. *Paper 79-23*, 1– 20.

Münchow, A., Kelly, K., Falkner, K.K., Melling, H., 2015. Baffin island and west Greenland current systems in northern Baffin Bay. Prog. Oceanogr. 132, 305–337. https://doi.org/10.1016/j.pocean.2014.04.001.

Newton, A.M.W., Knutz, P.C., Huuse, M., Gannon, P., Brocklehurst, S.H., Clausen, O.R., Gong, Y., 2017. Ice stream reorganization and glacial retreat on the northwest Greenland shelf. Geophys. Res. Lett. 44, 7826–7835. https://doi.org/10.1002/2017GL073690.

NGRIP community members, 2004. High-resolution record of Northern Hemisphere climate extending into the last interglacial period. Nature 431 (7005), 147–151. https://doi.org/10.1038/nature02805.

Ó Cofaigh, C., Dowdeswell, J.A., Jennings, A.E., Hogan, K.A., Kilfeather, A., Hiemstra, J. F., Noormets, R., Evans, J., McCarthy, D.J., Andrews, J.T., Lloyd, J.M., Moros, M., 2013. An extensive and dynamic ice sheet on the west Greenland shelf during the last glacial cycle. Geology 41, 219–222. https://doi.org/10.1130/G33759.1.

Okuma, E., Hingst, J., Weiser, Madaj, L., Titschack, J., Vogt, C., Kienast, M., Hillaire-Marcel, C., Dierk Hebbeln, D., Kasemann, S.A., 2023. Deglacial and Holocene sediment dynamics and provenances off Lancaster Sound: implications for paleoenvironmental conditions in northern Baffin Bay. Quat. Sci. Rev. 309, 108101. https://doi.org/10.1016/j.quascirev.2023.108101.

Okuma, E., Titschack, J., Weiser, J., et al., 2024. Shifting sediment depocenters track ice-margin retreat in Baffin Bay. Comm. Earth. Environ. 5 (1), 224. https://doi.org/10.1038/s43247-024-01393-9.

Ownsworth, E., Selby, D., Lloyd, J., Knutz, P., Szidat, S., Andrews, J., Ó Cofaigh, C., 2023. Tracking sediment delivery to central Baffin Bay during the past 40 kyrs: insights from a multiproxy approach and new age model. Quat. Sci. Rev. 308, 108082. https://doi.org/10.1016/j.quascirev.2023.108082.

Pieńkowski, A.J., Coulthard, R.D., Furze, M.F.A., 2022. Revised marine reservoir offset (ΔR) values for molluscs and marine mammals from Arctic North America. Boreas 52 (2), 145–157. https://doi.org/10.1111/bor.12606.

Pieńkowski, A.J., England, J.H., Furze, M.F.A., Blasco, S., Mudie, P.J., MacLean, B., 2013. 11,000 years of environmental change in the Northwest Passage: a multiproxy core record from central Parry Channel, Canadian High Arctic. Mar. Geol. 341, 68–85. https://doi.org/10.1016/j.margeo.2013.04.008.

Pieńkowski, A.J., England, J.H., Furze, M.F.A., MacLean, B., Blasco, S., 2014. The late quaternary environmental evolution of marine arctic Canada: Barrow Strait to lancaster Sound. Quat. Sci. Rev. 91, 184–203. https://doi.org/10.1016/j.quascirev.2013.09.025.

Pieńkowski, A.J., England, J.H., Furze, M.F.A., Marret, F., Eynaud, F., Vilks, G., Maclean, B., Blasco, S., Scourse, J.D., 2012. The deglacial to postglacial marine environments of SE Barrow Strait, Canadian Arctic Archipelago. Boreas 41 (2), 141–179. https://doi.org/10.1111/j.1502-3885.2011.00227.x.

Rashid, H., Piper, D.J.W., Drapeau, J., Marin, C., Smith, M.E., 2019. Sedimentology and history of sediment sources to the NW Labrador Sea during the past glacial cycle. Quat. Sci. Rev. 221, 105880. https://doi.org/10.1016/J.QUASCIREV.2019.105880.

Rasmussen, S.O. Andersen, Svensson, K.K., Steffensen, A.M., Vinther, J.P., Clausen, B.M., Siggaard-Andersen, H.B., Johnsen, M.-L., Larsen, S.J., Dahl-Jensen, L.B., Bigler, D., Röthlisberger, M., Fischer, R., Goto-Azuma, H., Hansson, K., Ruth, M.E., 2006. A new Greenland ice core chronology for the last glacial termination. J. Geophys. Res. 111, D06102. https://doi.org/10.1029/2005JD006079, 2006.

Scambos, T.A., Bell, R.E., Alley, R.B., Anandakrishnan, S., Bromwich, D.H., Brunt, K., Christianson, K., Creyts, T., Das, S.B., DeConto, R., Dutrieux, P., Fricker, H.A., Holland, D., MacGregor, J., Medley, B., Nicolas, J.P., Pollard, D., Siegfried, M.R., Smith, A.M., Steig, E.J., Trusel, L.D., Vaughan, D.G., Yager, P.L., 2017. How much, how fast?: a science review and outlook for research on the instability of Antarctica's Thwaites Glacier in the 21st century. Global Planet. Change 153, 16–34. https://doi.org/10.1016/j.gloplacha.2017.04.008.

Shaw, J., Piper, D.J.W., Fader, G.B.J., King, E.L., Todd, B.J., Bell, T., Batterson, M.J., Liverman, D.G.E., 2006. A conceptual model of the glaciation of Atlantic Canada. Quat. Sci. Rev. 25, 2059–2081. https://doi.org/10.1016/j.quascirev.2006.03.002.

Sheldon, C., Jennings, A., Andrews, J.T., Ó Cofaigh, C., Hogan, K., Dowdeswell, J.A., Seidenkrantz, M.S., 2016. Ice stream retreat following the LGM and onset of the west Greenland current in Uummannaq Trough, west Greenland. Quat. Sci. Rev. 147, 27–46. https://doi.org/10.1016/j.quascirev.2016.01.019.

Simon, Q., Hillaire-Marcel, C., St-Onge, G., Andrews, J.T., 2014. North-eastern Laurentide, western Greenland and southern Innuitian ice stream dynamics during the last glacial cycle. J. Quat. Sci. 29, 14–26. https://doi.org/10.1002/jqs.2648.

Simon, Q., St-Onge, G., Hillaire-Marcel, C., 2012. Late Quaternary chronostratigraphic framework of deep Baffin Bay glaciomarine sediments from high-resolution paleomagnetic data. G-cubed 13, 1–24. https://doi.org/10.1029/2012GC004272.

Simon, Q., Thouveny, N., Bourles, D.L., Nuttin, L., Hillaire-Marcel, C., St-Onge, G., 2016. Authigenic 10Be/9Be ratios and 10Be-fluxes (230Thxs-normalized) in central Baffin Bay sediments during the last glacial cycle: paleoenvironmental implications. Quat. Sci. Rev. 140, 142–162. https://doi.org/10.1016/j.quascirev.2016.03.027.

Stanford, J.D., Hemmingway, R., Rohling, E.J., Challenor, P.G., Medina-Elizalde, M., Lester, A.J., 2011. Sea-level probability for the last deglaciation: a statistical analysis of far-field records. Global Planet. Change 79, 193–203. https://doi.org/10.1016/j.gloplacha.2010.11.002.

Tang, C., Ross, C., Yao, T., Petrie, B., Detracey, B., Dunlap, E., 2004. The circulation, water masses and sea-ice of Baffin Bay. Prog. Oceanogr. 63 (4), 183–228. https://doi.org/10.1016/j.pocean.2004.09.005.

Tippett, C.R., 1985. Glacial dispersal train of Paleozoic erratics, central Baffin Island, N. W.T., Canada. Can. J. Earth Sci. 22, 1818–1826.

Tremblay, T., Lamothe, M., 2022. New contributions to the ice-flow chronology in the Boothia-Lancaster Ice Stream catchment area. Geological Survey of Canada 6, 40. https://doi.org/10.4095/331062. Preprint.

Vaughan, J., England, J.H., Coulthard, R.D., La Farge, C., 2024. Passage and removal of the Amundsen Gulf Ice Stream, NW Laurentide Ice Sheet, recorded by the glacial and sea level history of southern Banks Island, Arctic Canada. Quat. Sci. Rev. 344, 10880. https://doi.org/10.1016/j.quascirev.2024.108880.

Vilks, G., 1980. Postglacial Basin Sedimentation on Labrador Shelf. Geological Survey Paper 78-28, p. 17.